

Ben-Gurion University of the Negev The Faculty of Natural Sciences The Department of **Physics**

Optical Clock Laser Stabilization and Frequency Dissemination

Yotam Weber

Thesis submitted in partial fulfillment of the requirements for the Master of Sciences degree

Under the supervision of Prof. Ron Folman

August, 2024



אוניברסיטת בן־גוריון בנגב הפקולטה למדעי הטבע המחלקה לפיזיקה

ייצוב לייזר שעון והפצת תדרים

יותם ובר

חיבור לשם קבלת התואר "מגיסטר" בפקולטה למדעי הטבע

בהנחיית פרופסור רון פולמן

אב תשפ"ד



Ben-Gurion University of the Negev The Faculty of Natural Sciences The Department of **Pysics**

Optical Clock Laser Stabilization and Frequency Dissemination

Yotam Weber

Thesis submitted in partial fulfillment of the requirements for the Master of Sciences degree

Under the supervision of Prof. Ron Folman

Signature of student:	Date:	30.8.2024
Signature of supervisor:	Date:	30.8.2024
Signature of chairperson of the		
committee for graduate studies:	Date:	

August, 2024

תקציר

מאז שחר הציוילזציה, היה לאנושות עניין במדידת זמן. לאורך השנים, מדידות הזמן התקדמו מעקיבה אחרי מחזור השמש בעזרת שעון שמש לשעוני מטוטלת. בעת המודרנית, שעוני יד משתמשים בגבישי קוורץ למדידת זמן עם דיוק ויציבות טובים יותר המתאפשרים משיפורים טכנולוגיים.

בימים אלו שעונים אטומים אופטיים משמשים למדידות הזמן המדויקות ביותר, עם שיפור של שלושה סדרי גודל לעומת שעונים אטומים בתחום המיקרוגל. שעוני המיקרוגל פותחו במאה העשרים וכיום משמשים להגדרת השניה.

הבסיס של כל שעון אטומי הוא יסוד אטומי בעל מעבר אנרגיות המאופיין בזמן חיים ארוך המאפשר זמני חקירה ארוכים. במעבדה שלנו, השעון מבוסס על איזוטופ 171 של יסוד האיטרביום. למעבר השעון באיטרביום אורך גל של 578 ננומטר ורוחב ספקטרלי של כעשרה מיליהרץ. האטומים מקוררים לטמפרטוה קרובה לאפס המוחלט ונלכדים על ידי מלכודת אופטית מחזורית הנקראת סריג אופטי כדי להתנגד לתאוצה הגרביטציונית. המלכודת מאפשרת לחקור מספר רב של אטומים לזמן ממושך בשביל מדידה עם אי ודאות סטטיסטית קטנה.

כדי לאפשר מדידה מדויקת של תדרים בתחום האופטי מספר התקדמויות טכנולוגיות נדרשו, בעיקר בתחום הלייזרים צרי־סרט וההמצאה של מסרק התדרים המאפשר להעביר את היציבות של תדר השעון לתדרים נמוכים יותר המאפשרים עיבוד על ידי אלקטרוניקה. הממציאים של מסרק התדרים, הול והאנץ' זכו על המצאה זו בפרס נובל בשנת 2005.

היכולות האלו של שעונים אטומיים אופטיים הופכות אותם למכשירי המדידה הטובים ביותר עבור מטרולוגיה, בחינת ניבויים של תורת היחסות ובדיקת

היסודות של מכניקת הקוונטים.

Abstract

Since the beginning of civilization, humanity has had an interest in measuring time. Over the years, time measurements have ranged from day and night tracking using sundials, to pendulum clocks, to modern wrist watches. These use quartz crystals to measure time, with the higher accuracy and precision made available by technological improvements. Atomic clocks enable accurate time and position management using satellite-based systems, such as the GPS (Global Positioning System).

Currently, optical atomic clocks are used to perform the best time measurements with a relative uncertainty of 10^{-18} and lower [1], an improvement of 3 orders of magnitude over the microwave atomic clocks developed in the 20th century and currently used as the definition of the SI second.

At the basis of every atomic clock stands an atomic species that possesses a metastable clock transition allowing long interrogation times. In the clock being developed in our lab, we use Ytterbium (Yb)-171 neutral atoms, which can be cooled to about 10 μ K to reduce their thermal velocity, as well as to enable trapping, thereby counteracting gravity. This is accomplished with a periodic optical potential called an optical lattice. Our aim is to achieve a long interrogation time of a large number of atoms for measurement with a small statistical uncertainty. The clock transition is ${}^1S_0 \longrightarrow {}^3P_0$ at 578 nm with a spectral width of less than 10 mHz [2].

To be able to realize and measure a frequency such as a clock reference, several technological advances are needed to occur, mainly improvements in laser technology which enable very narrow-linewidth lasers, and the

optical frequency comb allowing the transfer of the stability of the high frequency clock transition (~ 500 THz) to a low-frequency comb parameters [in the radio frequency (RF) spectrum] manageable by electronics. The frequency comb granted its inventors, John L.Hall and Theodor W. Hänsch, the 2005 Nobel prize [3].

These properties of optical atomic clocks make them the best measuring devices available for metrology, and even to experimentally explore theoretical predictions of General Relativity [4, 5] and the foundations of Quantum Mechanics [6, 7].

In this thesis, I provide a detailed description of the work that I have done on the ¹⁷¹Yb clock. Specifically, I contributed to the design and construction of the clock laser and cavity optical systems (see Fig. 3.4 and 3.3), the operation and locking of the clock laser and frequency comb, the implementation of the mini-link fiber stabilization, and the design and application of the frequency dissemination system (see Fig. 3.13).

Acknowledgements

First, I would like to express my deepest gratitude to my adviser, Prof. Ron Folman, for giving me the opportunity to study under his guidance. His insights, encouragement and support have been invaluable throughout this journey.

I am also immensely grateful to the entire clock team for their collective efforts and collaboration. In particular, I would like to thank the lab manager, Dr. David Grosswaser, for his guidance and assistance. His expertise and advice have been crucial in navigating the complexities of my research. A heartfelt thanks to Prof. Eli Sarid for the tremendous help in writing this document. Your feedback, suggestions, and support have been instrumental in shaping this thesis into its final form. I also extend my appreciation to my colleague, Yoseph, for his collaboration and support.

Special thanks to Yali and Yiftach for the time spent working alongside me in the lab and in classes. Your friendship and dedication have made the lab experience both productive and enjoyable. Additionally, I am grateful to Yaniv for his technical support and for creating a positive atmosphere in the lab. I would like to extend my sincere appreciation to the entire atom chip group for their contributions and support.

To my family, thank you for your unwavering support and encouragement. Your love and belief in me have been a constant source of strength. Lastly, to my girlfriend, Shani, thank you for your endless support, patience, and understanding. Your encouragement has been a cornerstone

in helping me persevere through the challenges of this journey.

Contents

A	bstra	ct		i
A	cknov	wlegem	ents	v
Li	st of	Figures		viii
Li	st of	Abbrev	iations	xi
1	Intr	oductio	on - Optical Lattice Clock	1
	1.1	Time a	and Frequency Measurements	1
	1.2	Optica	al Atomic Clocks	3
	1.3	.3 Comparisons and Dissemination of Optical Frequency St		
		dards		5
		1.3.1	Various Optical Frequency Standards	6
		1.3.2	Dissemination	7
2 Backgro		kgroun	d	9
	2.1 Yb Optical Atomic Clock		tical Atomic Clock	9
		2.1.1	Energy Levels	10
		2.1.2	Cooling Scheme	11
		2.1.3	Magic Frequency	13

CONTENTS

	2.2	Clock Laser Stabilization		
		2.2.1	Optical Cavity	15
		2.2.2	Pound-Drever-Hall (PDH) Technique	17
		2.2.3	Servo Bandwidth	21
	2.3	Optica	Optical Frequency Comb (OFC)	
		2.3.1	Carrier Envelope Offset (CEO) and Repetition Rate	
			Stabilization	23
	2.4	Stabili	zation of Optical Links	25
		2.4.1	Optical Fiber Noise	25
3	Exp	erimen	tal Realization of the Yb Clock System	29
	3.1	BGU Y	Yb Clock Setup	29
	3.2	Clock	Laser Lock Scheme and Operation	30
		3.2.1	Evaluation of the Cavity Finesse	37
		3.2.2	Comparison to an Independent Stable Laser System .	39
		3.2.3	Cavity Mini-Link	40
	3.3			42
		3.3.1	Lock to a Radio Frequency Reference	43
	3.4	Long-	Distance Fiber link Noise Cancellation System	44
4	Sun	ımary a	and Outlook	48
		-		
Bi	ibliography 5			50

List of Figures

1.1	Atomic clocks over the years	4
1.2	Israeli optical fiber network	7
2.1	Yb energy levels	11
2.2	Operation of an optical cavity	17
2.3	Pound-Drever-Hall (PDH) basic setup	19
2.4	Simulation of the PDH error signal	20
2.5	Principle of a frequency comb	22
2.6	Phase noise effect on an ideal oscillator	26
2.7	Fiber noise cancellation (FNC) scheme	27
3.1	BGU optical lattice clock block diagram	30
3.2	MOGLabs cateye configuration	31
3.3	Clock laser optical system	32
3.4	Cavity optical system	33
3.5	Cavity intensity monitoring	34
3.6	Ultra low expansion (ULE) cavity alignment and sidebands generation	36
3.7	PDH electronic eystem	37
3.8	Cavity Ring-down measurement	38

LIST OF FIGURES

3.9	Comparison to an independent stable laser system	39
3.10	Application of the Mini-link noise cancellation system	41
3.11	The optical frequency comb (OFC) system	42
3.12	Frequency comb lock to an RF signal	43
3.13	BGU fiber link noise cancellation system	45
3.14	BGU-TAU link block diagram	46

List of Abbreviations

ADEV Allen deviation

ADM add-drop multiplexer

AOM acousto-optic modulator

BBR black body radiation

BDU beat detection unit

CEO carrier envelope offset

DDS direct digital synthesis

DM dichroic mirror

ECDL external cavity diode laser

EOM electro-optical modulator

FI Faraday isolator

FNC fiber noise cancellation

FP Fabry-Perot

FSC fast servo controller

FSR free spectral range

GTP Glan-Thompson polarizer

MOT magneto-optical trap

NIR near-infrared

OFC optical frequency comb

OLC optical lattice clock

PBS polarizing beam splitter

PD photo-diode

PDH Pound-Drever-Hall

PID proportional integral derivative

PPLN periodically poled lithium niobate

QPN quantum projection noise

RF radio frequency

SHG second harmonic generation

SI International System of Units

ULE ultra low expansion

Yb Ytterbium

1 Introduction - Optical Lattice Clock

1.1 Time and Frequency Measurements

Time measurements have evolved enormously throughout history. Early humans relied on astronomical phenomena, such as the movement of the sun and the changing seasons, to gauge time. Sundials were among the first tools to measure time more accurately. The invention of mechanical clocks in the Middle Ages marked a significant advancement, enabling more precise timekeeping and fostering the growth of trade and industry. The pendulum clock, developed in the 17th century, further refined the accuracy of time. The 20th century brought about the the first electronic clocks, based on the frequency of a quartz oscillator, which uses vibrations of quartz crystals to measure time with higher precision and smaller size. The invention of atomic clocks that measure the microwave radiation frequency required to excite energy levels in atoms was the next step towards more accurate timekeeping. Such a microwave transition of the Cs atom has been used since 1967 as the definition of the International System of Units (SI) second.

The setup of every atomic clock contains a local oscillator that drives a population change of the atomic energy levels using a narrow atomic transition. The population change is measured to produce a correction signal to lock the local oscillator frequency, thus achieving a stable frequency reference. In the past, the transitions used by the first atomic clocks were the microwave frequency of the ground-state hyperfine splitting of alkali

metals. Currently, Cs fountain clocks are at the pinnacle of accuracy for microwave atomic clocks, with a fractional uncertainty of 10^{-15} and lower [8].

The optical lattice clock (OLC), based on neutral atoms, is one of the main candidates (among other optical atomic clocks such as ion clocks) to lead the next stage of development in the field of precise time measurement and timekeeping. OLCs are projected to play a major role in the redefinition of the SI second with optical frequencies [9, 10].

The quality of a clock (or frequency standard) is determined by two main parameters: firstly, its systematic uncertainty or accuracy; the possible deviation of the measured frequency from the known unperturbed value. Systematic uncertainty is determined by experimental factors such as atomic level shifts caused by black body radiation (BBR) originating in the enviorment [11] and by the light from the optical lattice holding the atoms [12]. Secondly, stability, that is, the statistical precision of the clock frequency measurements. The statistical instability is usually measured by Allen deviation (ADEV) - $\sigma(\tau)$ (named after D.W. Allen [13]). The ADEV is a mathematical tool that quantifies the correlation between consecutive measurement intervals τ . The Allen variance (the square of the ADEV) is given by [14]:

$$\sigma(\tau)^2 = \frac{1}{2(M-1)} \sum_{i=1}^{M-1} (\bar{y}_{i+1} - \bar{y}_i)^2, \tag{1.1}$$

where \bar{y}_i is the average value of the i-th fractional frequency values out of M values taken during the measurement interval τ . When using a frequency reference to stabilize the standard, such as a narrow atomic transition, the total stability can be estimated by [15, 16]:

$$\sigma(\tau) \propto \frac{1}{O} \frac{1}{S/N} \sqrt{\frac{T}{\tau}},$$
 (1.2)

where $Q = \nu/\Delta\nu$ is the quality factor of the atomic clock that depends on

the measurement technology used (for example, in a microwave fountain clock, using Ramsey interrogation, $\Delta \nu$ is $1/T_{Ramsey}$ [17]), S/N is the signal-to-noise ratio of the measurement and T is the single measurement cycle time. Under optimal conditions, the lower limit for the S/N is quantum projection noise (QPN) [18, 19] also known as the "Standard Quantum Limit" of:

$$S/N = \sqrt{N_{atom}},\tag{1.3}$$

where N_{atom} is the number of atoms in the interrogated population. For example, a state-of-the-art ¹³³Cs beam clock with $\nu = 9,192,263,770$ Hz, a narrow linewidth of 1 Hz and a population of 10^6 atoms, can reach an ADEV in the range of 10^{-13} after only 1 s averaging time [20], where a typical single measurement cycle time is on the order of 1 s.

1.2 Optical Atomic Clocks

The simplest way to achieve a clock with better stability, according to Eq. 1.2, is to improve the quality factor, for example by using higher frequencies without sacrificing the transition linewidth. Using optical instead of microwave frequencies as clock transitions gives a potential for five orders of magnitude improvement. Dipole-forbidden electronic transitions in the optical domain have very narrow linewidths, making them suitable for use as clock transitions. To realize the full potential, the rest of the parameters that affect instability need to be improved to the level of Cs fountain clocks, such as the number of interrogated atoms (a few thousands for OLCs).

All optical clocks share the same basic principles of operation. The local oscillator of the clock is established by frequency locking a laser to a high-finesse cavity, achieving short-term stability of the laser [21]. Simultaneously, the stable laser is used to probe the atomic population under test, creating a long-term frequency reference by tuning the laser frequency to the interrogated narrow atomic resonance.

Fig. 1.1 shows the stability values of microwave and optical references achieved over the last three decades. Rapid improvements in optical clocks has been enabled by the development of atom manipulation technologies such as laser cooling and trapping, and by the invention of the optical frequency comb.

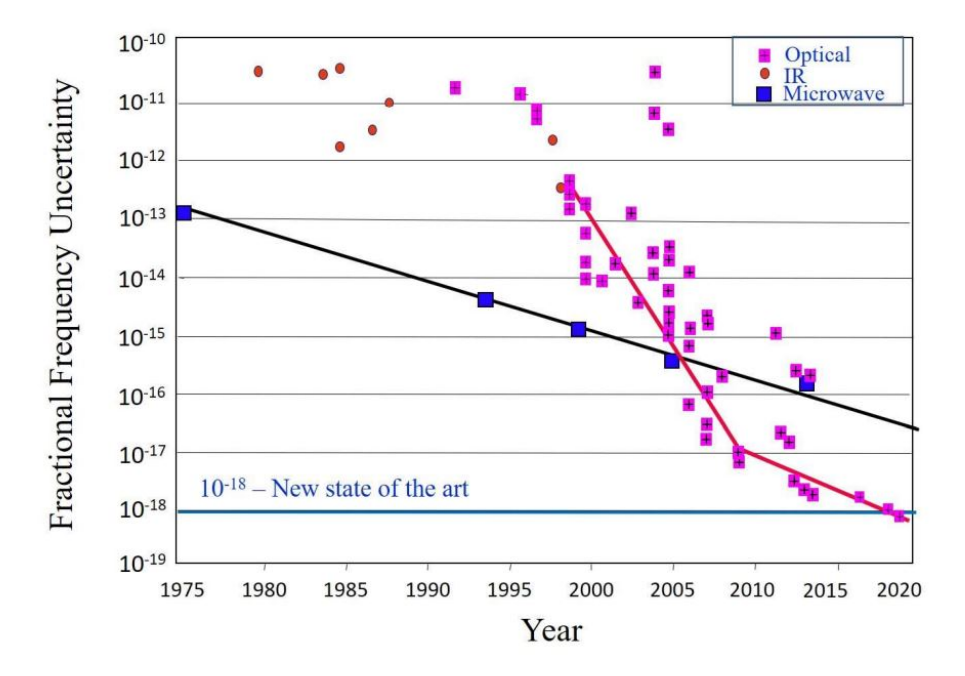


Figure 1.1: Progress in the long-range fractional uncertainty achieved by atomic clocks [22]. While Cs fountain microwave clocks have steadily improved since their emergence, the invention of the frequency comb enabled optical standards like the trapped ion and OLCs to take the lead as the best frequency standards with a fractional uncertainty of $\sim 10^{-18}$ and lower [23].

There are two main realizations of optical atomic clocks: charged ion clocks and neutral-atom OLCs. Work is also being done towards the realization of a nuclear optical clock using a thoriom-229 nuclei [24], with promising potential, but such a clock has not yet been built. Additionally, several groups are developing optical clocks using diatomic molecules of iodine [25] and strontium [26]. Another "exotic" optical clock is being developed using a continuous-wave atom laser [27].

Optical ion clocks are usually based on a single ion trapped and cooled

by electric fields (both static and oscillating) and laser radiation, respectively. Neutral atoms cannot be trapped by electric fields. To overcome this obstacle, the technique of optical dipole trapping [28] is being used in the form of an optical lattice (a spatially periodic dipole trap), with the added benefit of trapping and interrogating a large number of atoms simultaneously. Both approaches enable long interrogation times for the atomic species under test to allow high-precision spectroscopy. While ion clocks are realized with a simpler system, this comes at the cost of a few orders of magnitude lower signal-to-noise ratio due to the population size compared with OLCs.

We in the BGU Atom-Chip Group are working on a ¹⁷¹Yb OLC for future contributions to international frequency comparisons as well as for developing the potential for an independent and robust optical frequency standard local to Israel.

The ¹⁷¹Yb OLC is a very complex system consisting of several different lasers (for cooling, trapping, and interrogation of the atoms), as well as the frequency comb and an ultra-stable optical cavity. For a detailed explanation of the system, see Sec. 2.1.

1.3 Comparisons and Dissemination of Optical Frequency Standards

As the technology of optical frequency standards enabled improvement beyond the SI level - the accuracy of the definition of the second, a problem arose in determining the accuracy of optical clocks. One may ask: how can I know how accurate my clock is if it is more accurate than the current standard? The answer is to compare it with a clock showing similar capabilities. Comparisons can be made in the same lab with two independent clocks with identical or different atomic species, or with remote clocks via free-space or optical fiber links [29].

1.3.1 Various Optical Frequency Standards

Ytterbium (Yb)-171 OLCs were first developed in the USA in 2009 [30]. Recently, a group at NIST constructed a shallow lattice apparatus with the potential to achieve fractional uncertainty beyond the 10^{-18} level [12]. At INRIM in Italy, continuous operation of a Yb clock with sub-nanosecond capabilities was recently reported [31]. In Asia such clocks operate in Japan [32], China [33], and Korea [34]. Other neutral-atoms OLCs have been developed with ⁸⁷Sr [11, 35]. A recent publication from JILA demonstrates a clock with stability of 8×10^{-19} [23]. Other OLCs have been developed using ¹⁹⁹Hg [36, 37] and ¹⁹⁹Cd [38].

In Israel, a $^{88}\text{Sr}^+$ single ion optical clock is being developed at the Weizmann Institute. Other $^{88}\text{Sr}^+$ clocks have been developed in Germany [39] and Canada [40] with fractional uncertainty on the order of 10^{-17} . Various additional ionic species have been used for ion clocks, such as Yb⁺ [41], Hg⁺ [42], Ca⁺ [43]; Al⁺ has been used for an ion clock with systematic uncertainty of 9.4×10^{-19} and a frequency stability of $1.2 \times 10^{-15}/\sqrt{\tau}$ has been reported [44].

Currently, the dominant limiting factor in the absolute frequency measurement of the clock transitions of optical references is the inaccuracy of the definition of the SI second [45]. This raises interest in frequency ratio measurements between different atomic references. Together, three independent ratio measurements should satisfy the following loop closure relationship:

$$\frac{\nu_a}{\nu_b} \times \frac{\nu_b}{\nu_c} \times \frac{\nu_c}{\nu_a} = 1,\tag{1.4}$$

where v_i (i = a, b, c) are individual clock frequencies. Full loop closures have been demonstrated for 171 Yb/ 87 Sr/ 199 Hg up to 10^{-16} [46], and for 171 Yb/ 87 Sr/ 27 Al+ up to 10^{-19} [29].

1.3.2 Dissemination

The most common method used to distribute the optical clock signal is a long-distance optical fiber link. Usually, an existing communication fiber is used as the conduit for accurate frequency transfer between remote locations without the need for additional infrastructure.

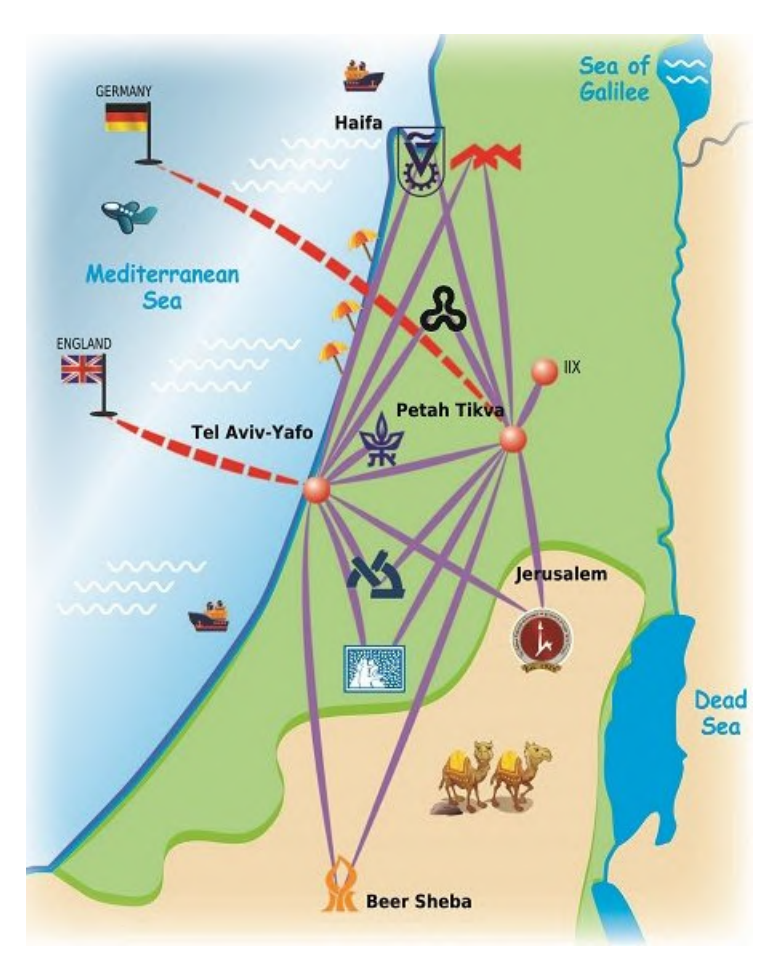


Figure 1.2: The communications fiber network connecting Israel's main universities [47]. The red dashed line represents two international links to the European GEANT network and through these to the American research network Internet2.

In Europe a vast network of fiber links has been established between most metrology institutes; in Switzerland, for example, connecting Bern, Basel and Zurich [48]; in Italy a 1739 km network spanning from Turin (INRIM) in the north to Matera in the south [49]; in France, from Paris to Lille (225)

CHAPTER 1. INTRODUCTION - OPTICAL LATTICE CLOCK

km) and Strasbourg (705 km) [50]; and in Germany, from Hanover to Munich for a total of 930 km [51]. International networks are also in use; for example, from Turin to Paris [52] and between Braunschweig (PTB), Paris (SYRTE) and London (NPL), for a total of 2220 km [53].

Fig. 1.2 presents the layout of the fiber communication network connecting the main universities in Israel. Each institute is connected to the two central hubs, one in Tel Aviv and another in Petah Tikva. We plan to use the BGU-Tel Aviv-Weizmann link to compare our clock with the Weizmann $^{88}\text{Sr}^+$ ion clock.

2 Background

2.1 Yb Optical Atomic Clock

Ytterbium is an element from the lanthanide series of the periodic table with the atomic number 70. The $^{171}\mathrm{Yb}$ fermionic isotope is commonly chosen for OLCs because of its useful properties. Fermions are preferable to bosons to reduce the number of atoms at the same lattice site (only one in the case of a 3D lattice [54]), thereby minimizing the frequency shift caused by collisions. The $^{171}\mathrm{Yb}$ fermionic isotope has a narrow transition (<10 mHz [2]) in the optical domain (578 nm), suitable as a clock transition. Furthermore, $^{171}\mathrm{Yb}$ clocks benefit from the structure of accessible energy levels in the visible and near-infrared (NIR) spectral regions (see Fig. 2.1) to perform primary and secondary cooling. In addition, the $^{1}\mathrm{S}_{0} \rightarrow ^{3}\mathrm{P}_{0}$ clock transition exhibits a "magic wavelength" (759 nm) that allows the use of an optical lattice with a minimal AC Stark shift (see Sec. 2.1.3). Last, studies have shown that Yb clocks are relatively less sensitive to ambient temperature variations in terms of BBR compared to other atomic references [55].

2.1.1 Energy Levels

The 171 Yb clock transition (yellow arrow in Fig. 2.1) between the ground-level singlet state 1 S₀ and the excited triplet 3 P₀ state is a forbidden transition in terms of both spin ($\Delta S \neq 0$) and dipole ($J = 0 \rightarrow J' = 0$) selection rules [16]. Ytterbium-171 possesses the smallest possible non-zero nuclear spin I = 1/2, splitting the ground and exited states to two substates $m_F = \pm 1/2$ in an external magnetic field through the Zeeman effect. Theoretical studies have shown that introducing external fields increases the transition strengths without significant perturbations to the clock frequency [56]. Thus, having the lowest (non-zero) nuclear spin is beneficial for accurate optical spectroscopy while having a relatively simple level structure of only two substates per level, compared to nine for 87 Sr, for example [11].

The clock transition (578 nm) has the special attribute of a possible magic wavelength (λ_{magic} in Fig. 2.1) for trapping in an optical lattice, where the Stark effect shifts due to external electric fields at that frequency are equal for the ground state and the excited state, thus providing the ability to trap the atoms with minimal effect of the Stark shift on the clock frequency (see Sec. 2.1.3).

The other transitions presented are used for the preparation of the atoms. The ${}^1S_0 \rightarrow {}^1P_1$ transition (blue arrow in Fig. 2.1) at 399 nm is used for the initial stages of cooling (Zeeman slower and 2D MOT) and in the detection stage. Its wide linewidth of 29 MHz contributes to the high capture range of the 2D MOT (see the following section). The ${}^1S_0 \rightarrow {}^3P_1$ (green in Fig. 2.1) narrower transition at 556 nm with 182 kHz linewidth is used for the second-stage cooling, namely 3D MOT and spin polarization of the atomic population. To repump the population during the cooling and detection

¹Readers familiar with the energy levels of alkali metals will notice the lack of hyperfine splitting of the clock transition levels due to zero total angular momentum.

²The spectroscopic notation used in this text as follows: $^{2s+1}L_J$, where 2s+1 is the number of spin states, L is the state orbital angular momentum quantum number and J=L+s is the total angular momentum quantum number.

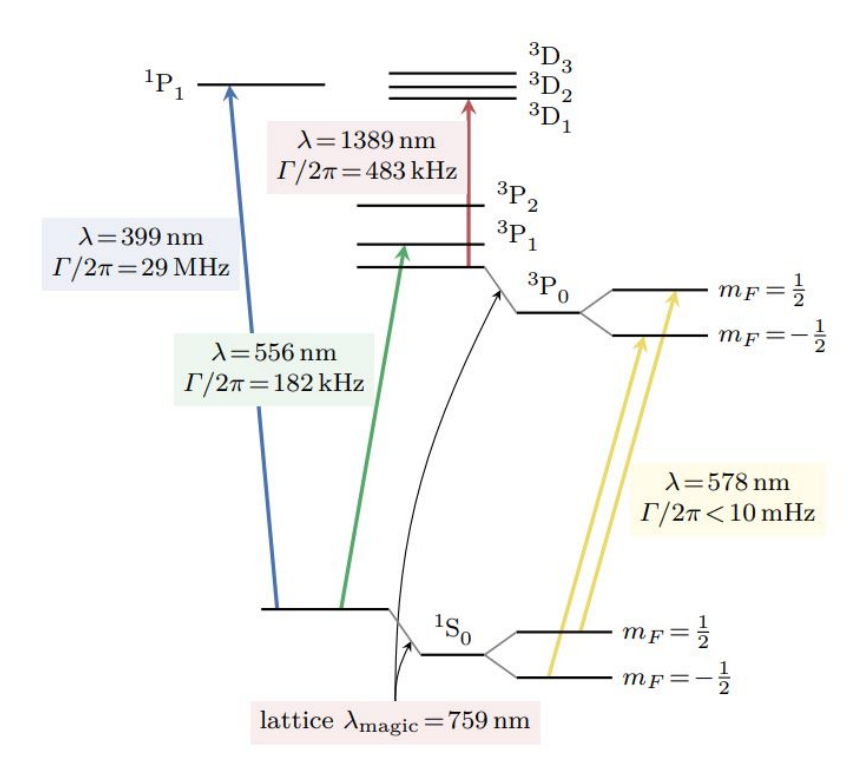


Figure 2.1: The relevant energy levels for 171 Yb, including the Zeeman splitting of the clock transition 1 S $_{0} \rightarrow ^{3}$ P $_{0}$ at 578 nm (yellow). The strong transition 1 S $_{0} \rightarrow ^{1}$ P $_{1}$ at 399 nm (blue) is used for the first-stage laser cooling [Zeeman slower and 2D magneto-optical trap (MOT)] and for detection of the atoms. The 1 S $_{0} \rightarrow ^{3}$ P $_{1}$ transition at 556 nm (green) is used for second-stage cooling (3D MOT) and spin polarization. To repump the population back to the ground level, the fast decaying 3 P $_{0} \rightarrow ^{3}$ D $_{1}$ level at 1389 nm (red) is used. The magic frequency of the clock transition 759 nm (black) is used to create the optical lattice trapping potential [2].

stages, the ${}^{3}P_{0} \rightarrow {}^{3}D_{1}$ transition at 1389 nm is used (red in Fig. 2.1).

2.1.2 Cooling Scheme

The setup of the complete cooling system is described in detail in [57]. First, the Yb source is heated inside an oven to ~ 700 K to produce a sufficiently high vapor pressure ($\sim 7 \times 10^{-4}$ Torr). Steel capillaries collimate the atomic flux from the oven to the center of the 2D MOT chamber. The hot atomic beam is then slowed by a Zeeman slower configuration [58], as explained below.

The hot atomic flux is illuminated by a 399 nm laser beam to slow the atoms on the way to the 2D MOT chamber. Using red-detuned light causes absorption of the counter-propagating photons (each with momentum $\hbar k$) and creates a maximal deceleration of $a_{max} = \hbar k \Gamma/2m$, the factor of 1/2 comes from the fact that half of the photons are emitted against the direction of the atomic beam, thus counteracting the deceleration. As the atoms slow down, the Doppler shift from resonance is reduced and the atoms go out of resonance with the illuminating beam. To compensate for this problem, a variable magnetic field operates along the atomic beam path to maintain the resonance between the slowed atoms and the red-shifted laser beam. The Zeeman slower tube in our system is designed to slow the atoms to a final velocity of 30 m/s at the center of the 2D MOT chamber from initial velocities of \sim 350 m/s [57].

Next, a 2D MOT is applied to further cool the atoms to $\sim 700~\mu\text{K}$ (in the two dimensions involved). The 2D MOT is realized by two sets of reddetuned counter-propagating laser beams with orthogonal circular polarizations (σ^+ , σ^- in the laboratory frame). Two sets of anti-Helmholtz coils generate the required magnetic field configuration: zero magnetic field along one axis (z) and a linear gradient along the remaining axes (x,y). The spatially dependent magnetic field causes the Zeeman splitting of the excited level into three sub-levels ($m_J = 0, \pm 1$). The polarization of the laser beams provides compliance with the selection rules, creating recoil for atoms propagating away from the center. The one-dimensional atomic beam is then pushed through a differential pumping tube to the lattice chamber using a pushing laser beam.

This intermediate cooling stage is important for two reasons: firstly, it reduces the background gas in the main science chamber and thereby lengthens the lattice lifetime; secondly, it eliminates the high BBR uncertainty caused by a "hot spot" from the oven, when directly viewed from the direction of the detection. In the lattice chamber, the atoms are loaded into a 3D MOT (at 556 nm) that cools the atoms to the 10 μ K temperature range. After these two stages of cooling, the atoms are cold enough to be

loaded into our optical lattice potential.

2.1.3 Magic Frequency

An optical lattice potential is a spatially periodic light intensity pattern caused by a standing wave formed by two counter-propagating laser beams or a cavity. The interaction of the induced dipole of the atoms with the oscillating electric field creates the potential suitable for an optical trap. Neutral atoms in the presence of laser light with intensity I and frequency ω experience the following dipole force [28]:

$$\vec{F} = \frac{1}{2\epsilon_0 c} \alpha_i(\omega) \vec{\nabla} I, \qquad (2.1)$$

where ϵ_0 is the vacuum permittivity, c is the speed of light, and α_i is the real part of the induced polarizability, which depends on the detuning of the laser frequency relative to a resonance transition frequency between two atomic levels. The force is directed toward electric-field maxima for red-detuning and towards electric-field minima for blue-detuning. A focused laser beam can trap a large number of atoms at high densities, but interactions and collisions between atoms will damage the clock performance. A preferred method is to load low-density atomic samples into an optical lattice potential created at the waist of a standing wave to maximize the laser intensity and phase-front stability. The small number of atoms in each lattice site in this situation lowers the collision probability, significantly reducing the clock uncertainty.

The standing wave forming the optical lattice induces a time- and position-dependent AC Stark shift, perturbing the clock transition. The frequency shift in state $|i\rangle$ induced by a field with amplitude E_0 is given by:

$$\Delta\omega_i = -\frac{1}{2\hbar}\alpha_i(\omega, \vec{e})E_0^2, \qquad (2.2)$$

where \vec{e} is the direction of the polarizability. The frequency difference between the clock states becomes [59]

$$\tilde{\omega}_{eg} = \omega_{eg} - \frac{1}{2\hbar} \Delta \alpha_{eg}(\omega, \vec{e}) E_0^2 + O(E_0^4), \tag{2.3}$$

where $\Delta\alpha_{eg}=\alpha_e-\alpha_g$ is the difference of dipole polarizabilities. It is impossible to maintain a stable laser intensity to ensure this shift remains constant over time. Thus, to cancel the time dependence of this expression, the lattice frequency must be tuned to eliminate the polarizability difference [60, 61]. For the ¹⁷¹Yb clock states, tuning to a "magic wavelength" of 759.35596 nm leads to $\Delta\alpha_{eg}=0$ [62, 63]. The scalar nature of the clock states (J=0) gives negligible dependence on the polarization of the lattice light and the polarizability dependency on \vec{e} can be dropped.

The optical lattice provides the ability to trap thousands of atoms in thousands of lattice sites for prolonged periods of time, achieving a high S/N ratio.

In addition, the atoms trapped in the lattice can be cooled by sideband cooling. The attractive potential of a 1D lattice is given by

$$U(z,\rho) = -U_0 \cos^2\left(\frac{2\pi z}{\lambda}\right) \exp\left\{-\frac{2\rho^2}{\rho_0^2}\right\},\tag{2.4}$$

where z and ρ are longitudinal and radial coordinates, U_0 is the depth of the trap in the center of the Gaussian beam (ρ , z=0) and ρ_0 is the radius of the beam at the waist. This potential can be approximated (at the antinodes of the standing wave) as a two-dimensional harmonic oscillator:

$$U(z,\rho) \approx U_0 \left[\left(\frac{2\pi z}{\lambda} \right)^2 + \frac{2\rho^2}{\rho_0^2} \right] = \frac{1}{2} m \omega_z^2 z^2 + \frac{1}{2} m \omega_\rho^2 \rho^2,$$
 (2.5)

with $\omega_z \equiv \frac{2\pi}{\lambda} \sqrt{\frac{2U_o}{m}}$ and $\omega_\rho \equiv \frac{2\pi}{\rho_0} \sqrt{\frac{2U_o}{m}}$, where m is the mass of the atom. The intensity variations along the longitudinal z axis are much more significant compared with the transverse radial direction. The resulting energy levels are as follows:

$$E_n = \hbar \omega_z \left(n + \frac{1}{2} \right), \quad n \in \mathbb{N}.$$
 (2.6)

Thus, the atomic wave function can be divided into two parts: the internal electronic wave function and the external vibrational part, which describes the motion in the lattice. This gives rise to vibrational transitions along with electronic ones $|g,n\rangle \to |e,m\rangle$ [for frequency $\omega_0 + (m-n)\omega_z$]. To realize the sideband cooling technique, a red-detuned laser pulse resonant with the transition $|g,n\rangle \to |e,n-1\rangle$ is applied. A second repumper pulse is applied, which transfers the atoms to a fast decaying state $|e,n-1\rangle \to |e',n-1\rangle$. The population will then spontaneously decay to the electronic ground state without a change in the vibrational level $|e',n-1\rangle \to |g,n-1\rangle$. As the atoms approach the vibrational ground state there is no excitation on the red sideband, resulting in reduced longitudinal temperatures of a few μ K. After sideband cooling, the atoms are ready to be interrogated by the clock laser (at 578 nm) and measured to complete the measurement cycle.

2.2 Clock Laser Stabilization

2.2.1 Optical Cavity

The Fabry-Perot (FP) resonator, also known as an optical cavity, is a set of two mirrors placed opposite to one another to form a standing wave with a frequency that matches the resonance condition [64]:

$$\nu = \frac{c}{2L} \cdot m = \nu_{FSR} \cdot m, m \in \mathbb{N}, \qquad (2.7)$$

where c is the speed of light, L is the length of the cavity, and v_{FSR} is the free spectral range (FSR), the frequency spacing between two adjacent resonances (or modes). This condition arises from the interference between beams that travel in opposite directions in the cavity. Taking into account

that the mirrors are not perfectly reflecting, we can define the reflection (and transmission) coefficient as the ratio between the reflected (and transmitted) electric field amplitude to the incoming amplitude:

$$r = \frac{E_{ref}}{E_{inc}} \quad , \quad t = \frac{E_{trans}}{E_{inc}}. \tag{2.8}$$

An incoming beam will be multiplied by r (or by t) each time it is reflected (or transmitted, respectively) from one of the mirrors, assuming both mirrors are the same. The total amplitude of the reflected field can be represented as a superposition of the light reflected from the cavity without entering, and the beams reflected from the cavity after completing any number of roundtrips, as seen in Fig. 2.2:

$$E_{ref}^{tot} = -E_{inc}r + E_{inc}\sum_{m=1}^{\infty}t^2r^{2m-1}e^{im2\Delta\varphi},$$
 (2.9)

where $\Delta \varphi = kL = \omega L/c$ is the phase accumulated while the beam propagates inside the cavity. Under the assumption of zero losses, we can apply $t^2 = 1 - r^2$ to Eq. 2.9 and calculate the sum as a geometric series to get:

$$E_{ref}^{tot} = \frac{r\left(e^{i2\Delta\varphi} - 1\right)}{1 - r^2 e^{i2\Delta\varphi}} E_{inc} = R(\omega) E_{inc}, \tag{2.10}$$

Calculating the reflected intensity gives the following equation:

$$I_{ref}^{tot} = I_0 \frac{4r^2 \sin^2(\Delta \varphi)}{t^4 + 4r^2 \sin^2(\Delta \varphi)} = I_0 \frac{\sin^2\left(\pi \frac{\nu}{\nu_{FSR}}\right)}{\left(\frac{\pi}{2F}\right)^2 + \sin^2\left(\pi \frac{\nu}{\nu_{FSR}}\right)},$$
 (2.11)

where \mathcal{F} is the finesse of the cavity defined as [64]:

$$\mathcal{F} = \frac{\pi r}{t^2} = \frac{\nu_{FSR}}{\delta \nu},\tag{2.12}$$

where δv is the linewidth of the resonator transmitted spectrum described by subtracting the reflected intensity (Eq. 2.11) from the incoming inten-

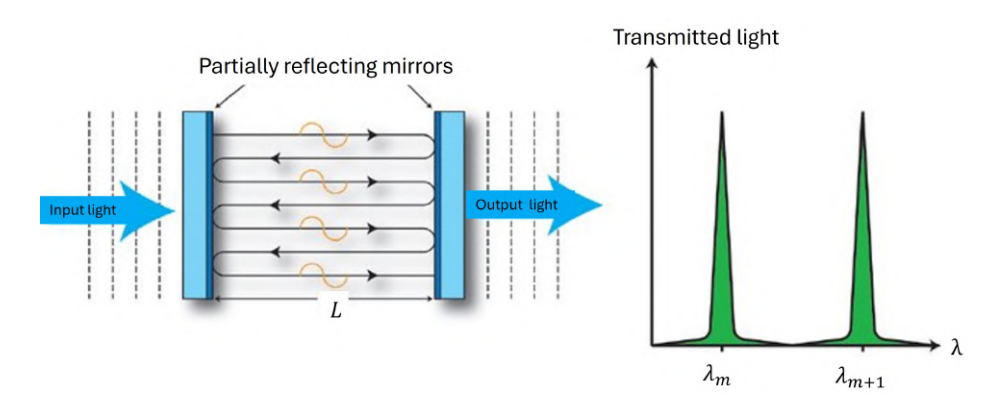


Figure 2.2: The operation principle of an optical cavity. Only light with the resonant condition (Eq. 2.7) of the FP resonator (normal modes of the cavity) can circulate inside the cavity and be transmitted through it, thus the cavity acts as a discrete frequency filter as shown on the right. The spectral width of the cavity is determined by the reflectivity of the mirrors constricting the cavity and can be expressed by the finesse parameter (Eq. 2.12) [65].

sity (assuming a no-loss cavity), and plotted in Fig. 2.2. Another interesting attribute of optical resonators is their ability to temporarily store resonance light intensity traveling between the mirrors. If the light is turned off the power inside the cavity will decay exponentially

$$I(t) = I_0 e^{-\frac{t}{\tau}},\tag{2.13}$$

where τ called the cavity lifetime given by [64]

$$\tau = \frac{L\mathcal{F}}{\pi c}.\tag{2.14}$$

Thus, measuring the decay time, known as a cavity ring-down measurement, can give a good estimate to the finesse of the cavity [66].

2.2.2 Pound-Drever-Hall (PDH) Technique

All lasers suffer from frequency fluctuations at different timescales that cause the broadening of the laser frequency spectrum. In the case of a diode laser (used in our system, see Fig. 3.2) for example, fast fluctuations are caused by statistical processes such as electron recombination, which

influence the refractive index and other parameters of the diode [67]. Slow fluctuations occur as a result of external perturbations, such as vibrations and temperature drifts. The linewidth of the laser can be reduced by the construction of a feedback loop. This would use an electronic servo to make corrections to the laser parameters according to the measured error signal, which is proportional to the difference between the desired laser frequency and the measured one.

Developed in the 1980's the PDH technique has become a commonly used method for locking the laser to a high-finesse optical cavity and achieving high-frequency stabilization [68–70]. The cavity resonances are detected by scanning the frequency of a laser and monitoring the transmission or reflection of the beam from the cavity. This signal is positive by definition, so it is not optimal as an error signal. The PDH technique described in Fig. 2.3 allows us to extract the phase of the complex reflection coefficient, which changes sign around the resonances to be used as the error signal.

The electric field of incident amplitude E_0 and frequency ω is phase modulated to:

$$E_{mod} = E_0 e^{i[\omega t + \beta \sin{(\Omega)}t]}, \qquad (2.15)$$

where β is the modulation depth and Ω is the modulation frequency. For small β the expression can be expanded to ³

$$E_{mod} \approx E_0 e^{i\omega t} [1 + i\beta \sin(\Omega)t] = E_0 e^{i\omega t} [1 + \frac{\beta}{2} e^{(i\Omega)t} - \frac{\beta}{2} e^{(-i\Omega)t}]. \quad (2.16)$$

This field consists of three components: two sidebands with detuning $\pm \Omega$ appear adjacent to the carrier frequency ω . The reflected field E_r from the cavity is given by:

$$E_r = E_0[R(\omega)e^{i\omega t} + \frac{\beta}{2}R(\omega + \Omega)e^{i(\omega + \Omega)t} - \frac{\beta}{2}R(\omega - \Omega)e^{i(\omega - \Omega)t}], \quad (2.17)$$

where $R(\omega) = \frac{E_r}{E_i}$ is the reflection coefficient of the cavity. The reflected

³A more rigorous approach uses the Jacobi-Anger expansion [72], with Bessel functions, but the following small-angle expansion is simpler and leads to the same result.

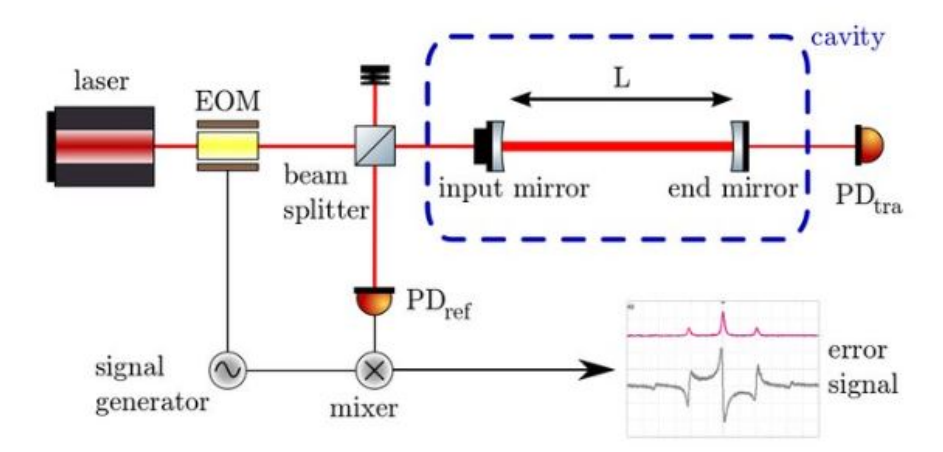


Figure 2.3: Description of the PDH setup: light from the laser is passed via an electro-optical modulator (EOM) into an FP resonator. The reflected light from the resonator is detected on a photo-diode (PD). The signal from the PD is mixed with the modulation signal and filtered. The resulting error signal, shown by the black line, serves as an input to a proportional integral derivative (PID) servo regulator, which keeps the laser frequency locked on the FP resonance. The red line depicts the transmission intensity of light through the cavity is presented. The frequency of the laser source is scanned to observe the transmission of the carrier and sidebands created by the EOM modulation [71].

power P_r which is measured by a photodetector (PD), is given by:

$$P_{r} = |E_{r}|^{2} = P_{0}|R(\omega)|^{2} + P_{0}\frac{\beta^{2}}{4}[|R(\omega + \Omega)|^{2} + |R(\omega - \Omega)|^{2}] + P_{0}\beta[\text{Re}\{(\chi(\omega))\}\cos(\Omega t) + \text{Im}\{(\chi(\omega))\}\sin(\Omega t)] + O(2\Omega),$$
(2.18)

where $P_0 = |E_0|^2$ is the power of the carrier, and where Re and Im denote the real and imaginary parts of χ , which is given by:

$$\chi = R(\omega)R^*(\omega + \Omega) - R^*(\omega)R(\omega - \Omega). \tag{2.19}$$

For a sufficiently high modulation frequency the sidebands will be totally reflected $[R(\omega \pm \Omega) \approx -1]$ because they are far away from the cavity resonance, so χ becomes purely imaginary:

$$\chi = -2i\operatorname{Im}\{R(\omega)\},\tag{2.20}$$

thus, the term oscillating at $\cos{(\Omega)}$ in Eq. 2.18 is cancelled, and we are left with the $\sin{(\Omega)}$ term oscillating proportionally to $\text{Im}\{R(\omega)\}$. This term is an asymmetrical function of $\omega-\omega_{res}$, the difference between the laser frequency and the resonance of the cavity. This sign-change around the resonance frequency allows us to use this term as the PDH error function.

The PD signal (the reflected power) is demodulated by multiplying it with a phase-delayed version of the original modulation frequency Ω . The mixer output then contains two terms, which are the sum and difference frequencies of the two input signals, so the signal of interest can be converted to a DC signal. This signal is passed through a low-pass filter to filter out the oscillating terms and obtain the PDH error signal.

A numerical simulation of the PDH error signal $(ImR(\omega))$ for different cavity finesse values is presented in Fig. 2.4. For this simulation the modulation frequency chosen is $\Omega=20$ MHz and the cavity FSR is 0.5 GHz. One can observe the effect of high finesse on the slope of the function at the locking point, allowing linewidth narrowing of the stabilized laser.

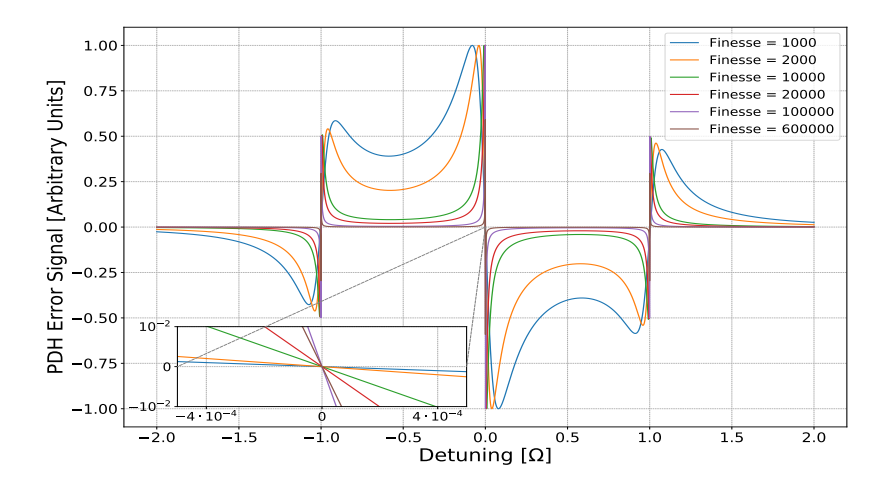


Figure 2.4: A simulation of the PDH error signal for different cavity finesse values. For all cases, the cavity length was 30 cm and $\Omega=20$ MHz. As can be seen, the higher the finesse of the cavity the sharper the fringes of the error signal. Thus, a steeper slope at the resonance locking point and a lower signal between the lock point and $\pm\Omega$ are obtained. Inset: expanded view of the locking point, clearly showing the steeper slope achieved for high-finesse values.

2.2.3 Servo Bandwidth

The Proportional-Integral-Derivative (PID) controller is a control algorithm widely used in engineering and industrial applications. It functions by calculating an error signal e(t) as the difference between a desired setpoint and the actual value of a process variable. The PID controller then uses this error signal to generate the control output u(t) that can help minimize the error and stabilize the system. u(t) has the form

$$u(t) = k_P e(t) + k_I \int_0^t e(\tau) d\tau + k_D \frac{de(t)}{dt},$$
 (2.21)

where $k_{P,I,D}$ is the gain parameter of the proportional, integral and derivative term, respectively. Adjusting the weights (k_P, k_I, k_D) of these three terms allows the PID controller to be tuned to achieve the desired system properties, such as stability, accuracy, and response speed. The proportional term contributes to the control output in proportion to the current error, the integral term helps to eliminate any residual error over time, and the derivative term predicts future errors based on the current rate of change.

The bandwidth is the range of frequencies over which the servo system can effectively control a process. Higher bandwidth indicates that the system can respond faster to changes in the input signal. This is particularly important in applications where speed and accuracy are crucial, such as laser stabilization. The total system bandwidth is composed of the controller bandwidth, the sampling rate at which the controller acquires the error signal, and the response of the system to the correction signal.

2.3 Optical Frequency Comb (OFC)

The development of OFCs revolutionized precision measurements in optics and lasers, affecting fields such as spectroscopy [73] and fundamental physics research [74], as well as telecommunications [75, 76]. Initially con-

ceptualized by Nobel laureates (2005)⁴ Theodor W. Hänsch and John L. Hall in the 1990s, OFCs have since evolved into indispensable tools across multiple disciplines.

At its core, an OFC is a device that produces a series of evenly spaced spectral lines spanning a broad range of frequencies within the electromagnetic spectrum, typically in the visible or infrared regime. These precisely spaced frequencies resemble the teeth of a comb, hence the name. What distinguishes OFCs is their exceptional coherence and stability, making them invaluable in numerous applications.

The generation of OFCs primarily relies on mode-locking of femtosecond lasers. Mode-locked lasers produce ultrashort pulses with extremely high and accurate repetition rates, resulting through Fourier transform in a highly precise comb-like frequency spectrum. Another technique for frequency comb generation is utilization of non-linear optical properties of microresonators to generate equally spaced spectral lines [77].

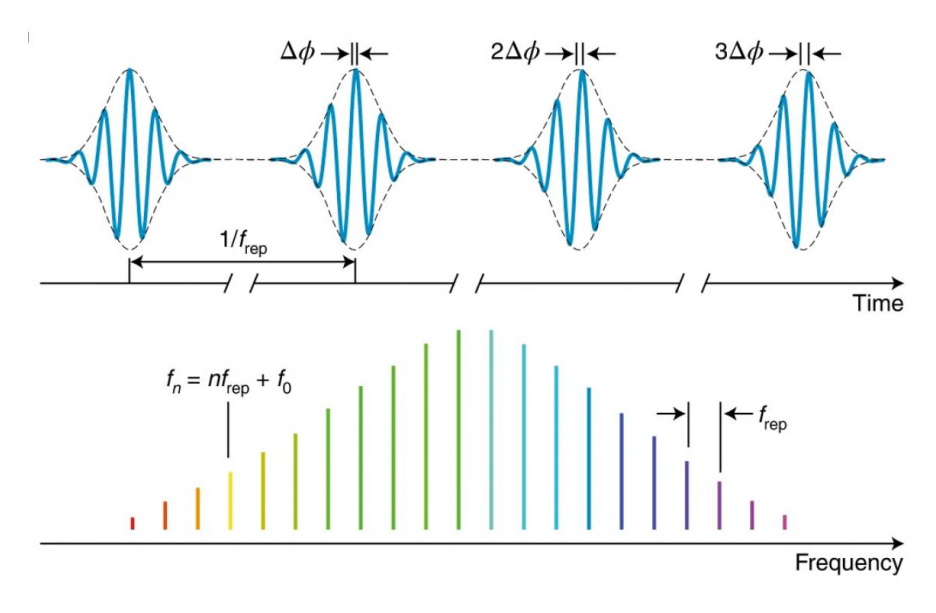


Figure 2.5: Top: time domain analysis of a mode-locked ultra-short pulse train with phase shift $\Delta \phi$ between the carrier and the envelope, and period between pulses $1/f_{rep}$. Bottom: the resulting frequency comb in the frequency domain, containing narrow spectral lines with shift $f_0 = f_{rep} \Delta \phi / 2\pi$ from their harmonic frequencies nf_{rep} [73].

⁴Shared with Roy J. Glauber for foundational work on quantum optics.

OFCs act as the "gears" of optical atomic clocks, correlating different optical frequencies and bridging the gap between different optical frequencies and between the optical and the micro-wave domains, thereby enabling the transfer of the clock information to much lower frequencies manageable by electronics, with no loss of precision. These unique properties have enabled breakthroughs in various fields. In telecommunications, OFCs facilitate high-speed data transmission over fiber-optic networks by precisely encoding information onto different frequencies. In spectroscopy, they enable ultra-high-resolution measurements, allowing scientists to probe molecular and atomic transitions with unprecedented precision. Furthermore, OFCs play a crucial role in the development of optical atomic clocks, which are essential for accurate timekeeping and navigation systems.

Using Fourier analysis from the time to the frequency domain, see Fig. 2.5, the pulses are translated into a discrete series of equally spaced sharp lines called teeth. The frequency of the n'th tooth is given by [16]:

$$f_n = n \cdot f_{rep} + f_{ceo}, \tag{2.22}$$

where f_{rep} is the repetition rate, the spacing between two consecutive teeth, and f_{ceo} (f_0 in Fig. 2.5) is the carrier envelope offset (CEO) frequency, which is the deviation of the comb teeth from an integer multiple of the repetition rate, caused by the phase difference between the carrier wave and the pulse envelope due to dispersion in the laser medium.

2.3.1 Carrier Envelope Offset (CEO) and Repetition Rate Stabilization

Both f_{rep} and f_{ceo} are radio frequencies (10s-100s MHz) that can be easily locked to a frequency standard (such as an Rb atomic clock in our laboratory) or, for higher accuracy, an optical reference (such as the clock laser in the optical atomic clock under development in our lab). Such locking

stabilizes the comb and in principle, makes each of its teeth an extremely stable, accurate and precise source of radiation. An absolute optical frequency can be achieved by measuring the beat note between the clock signal and the closest comb tooth. Locking of f_{ceo} is achieved by doubling the frequency of the n'th tooth of the low frequency part of the comb spectrum and comparing it to the 2n'th tooth of the high frequency part. The beat note of the two frequencies gives the offset frequency:

$$\begin{cases} f_n = f_{ceo} + n \cdot f_{rep} \\ f_{2n} = f_{ceo} + 2n \cdot f_{rep} \end{cases}$$

$$\implies 2 \cdot f_n - f_{2n} = 2(n \cdot f_{rep} + f_{ceo}) - (2n \cdot f_{rep} + f_{ceo}) = f_{ceo}.$$
(2.23)

This beat note can be phase locked to a stable RF source to lock the frequency shift of each comb tooth relative to the harmonic frequency $n \cdot f_{rep}$. The comb laser cavity properties (length and refraction index) determine the repetition rate. To stabilize the repetition rate, there are two options:

- 1. Locking to an RF signal the fourth harmonic of f_{rep} is compared with a signal synthesized from a frequency standard (Rb clock). The mixed signal phase is detected and sent into a servo driving the comb cavity piezo-electric actuator to complete the phase-locked loop.
- 2. Locking to an optical reference the beat note (f_{beat}) between the nearest comb tooth (f_m) to a stable optical reference with frequency f_{ref} is phase locked, thus transferring the stability of f_{ref} to every frequency component u:

$$m \cdot f_{rep} = f_{ref} - f_{ceo} + f_{beat}$$

$$\implies f_u = f_{ceo} + \frac{u}{m} (f_{ref} - f_{ceo} + f_{beat}).$$
(2.24)

Once both the repetition rate and carrier offset frequencies are stabilized to a frequency reference, its stability is coherently transferred to the entire spectral span of the comb.

Comparison of the comb with an external laser frequency is done using a beat detection unit (BDU), a device that creates spatial overlap between the comb and the external laser light. The comb light's broad spectrum is optically filtered to the specified frequency range, typically with a spectral width of 0.5 nm. The beat note between the laser and the adjacent comb tooth is measured while electronically filtering the beat notes with the other teeth at higher frequencies.

2.4 Stabilization of Optical Links

Stabilized laser systems are typically integrated in a tabletop configuration with multiple optical, electrical, and vacuum components, and consequently not portable. A preferred way to distribute optical standards is by an optical fiber. When propagating through the optical fiber, perturbations in the fiber medium cause phase noise in the optical signal and linewidth broadening.

2.4.1 Optical Fiber Noise

Optical fibers are subjected to thermal and acoustic effects that cause changes to the effective optical path length of the light propagating through them and, in turn, to the phase at their output. The phase accumulated in the fiber of length L is given by

$$\varphi = nk_0 L \equiv \beta L, \tag{2.25}$$

where n is the index of refraction and k_0 is the wavenumber, $k_0 = 2\pi/\lambda$. Thermal and mechanical fluctuations produce variations in the index of refraction through the thermo-optic effect and in the length of the fiber by thermal expansion and mechanical vibrations [78]. Thus, the phase variation takes the form

$$\Delta \varphi = \Delta \beta L + \beta \Delta L. \tag{2.26}$$

For an ideal oscillator this phase noise has a direct effect on the frequency noise and broadening of the linewidth, as demonstrated in Fig. 2.6.

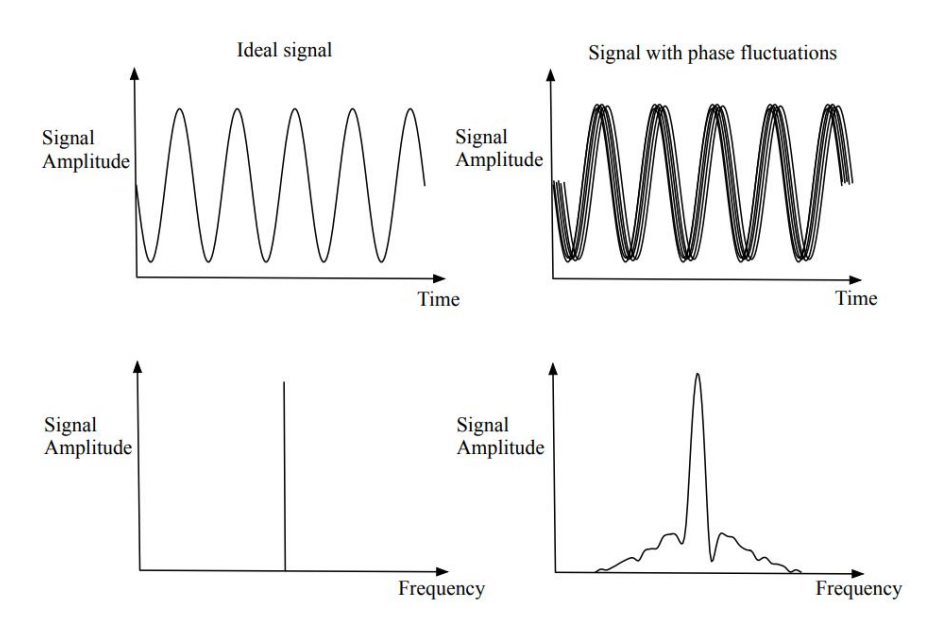


Figure 2.6: Time and frequency domain analysis of an ideal oscillator (left column) and one with phase fluctuation noise. In the frequency domain, the effect of the phase noise causes broadening of the spectral line and frequency noise [79].

To compensate for this noise, a system may be constructed, as first suggested in [80], using an acousto-optic modulator (AOM) to modulate the original signal. The fiber noise cancellation (FNC) system implemented in our setup is presented in Fig. 2.7. The AOM performs the measurement and cancellation of the phase accumulated along the optical path of the light through the fiber. In principle it is a variation of the Michelson interferometer, in which one arm with the original stable frequency interferes with the beam in the second arm, which is modulated and passes through the fiber. An AOM (AOM1) is used to shift the frequency of light from the base frequency ν_0 and is sent through the fiber. Part of the output light is modulated by AOM2 and retro-reflected back to the fiber. After a second pass through AOM1 the circulated beam frequency is

$$\nu = \nu_0 + 2(\Omega_1 + \Omega_2 + \delta_{\nu}), \tag{2.27}$$

where Ω_i are the modulation frequencies of AOMi and δ_{ν} is the noise accumulated through a one-directional passage through the fiber, assuming that the same phase noise is accumulated while passing through the fiber in both directions.

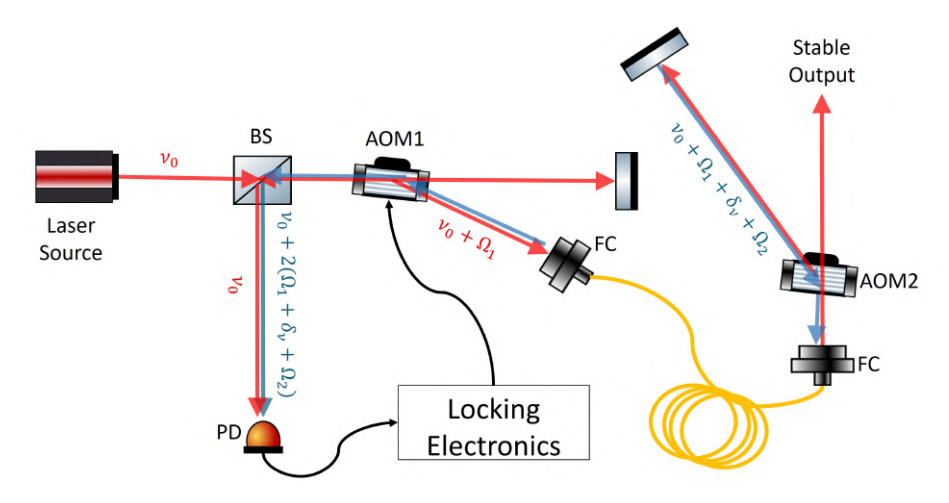


Figure 2.7: A general fiber link stabilization scheme. The first order diffracted beam from AOM1 (with modulation frequency Ω_1) propagates through the fiber to the link output. A portion of it is reflected back to the fiber, making a double pass through AOM2 (with modulation frequency Ω_2) and mixed after another pass through AOM1 with the zero-order beam (with frequency ν_0) - the lab arm of the interferometer. Thus the returned beam (blue) frequency is shifted twice by each AOM and by the noise induced by the fiber δ_{ν} , relative to the original laser frequency ν_0 . The locking electronics mix the beat note of the two arms of the interferometer with a stable RF source to create an error signal that drives AOM1 to reduce the noise. AOM - acousto-optic modulator, FC - fiber coupler, PD - photo-diode, BS - beam splitter. All graphical components are taken from [81].

The two arms of the interferometer are mixed and a PD measures the interference signal. The beat note is compared with a stable RF source to generate an error signal. The error signal is fed to a servo controller that modulates the AOM1 frequency to achieve a constant signal at the PD, thereby achieving a stabilized link. Having the second AOM2 enables us to differentiate between reflections along the optical path and the beam reflected from the mirror on the output side. Looking only at the light frequency that was also shifted by AOM2 ensures that we look at the light

that has probed the whole length of the fiber we aim to stabilize.

For this fiber noise cancellation (FNC) system to work, the roundtrip length of the optical (2L) fiber must be shorter than the coherence length (l_c) of the propagating photons, otherwise, no interference is possible. The coherence length is given by

$$l_c = \frac{c}{n\Delta \nu'},\tag{2.28}$$

where n is the index of refraction of the fiber medium, c is the speed of light, and Δv is the linewidth of the laser. For example, for a 1 Hz linewidth light, the coherence time is 1 second, and the coherence length is about 10^8 meters, about twice the circumference of Earth. For a 50 km fiber, you need the linewidth to be better than 1 kHz.

These kinds of stabilized fiber links are extremely sensitive to acoustic vibrations and have recently demonstrated their usefulness as sensors for seismic activity [82].

3 Experimental Realization of the Yb Clock System

3.1 BGU Yb Clock Setup

Fig. 3.1 shows a block diagram of the BGU Yb optical clock system. Each subsystem (block) will be explained in detail in the following sections, except for the cooling and measurement cycle block (upper-left corner), which is presented in [57].

The light of the clock laser (see Fig. 3.2) is divided into three branches (see Fig. 3.3). The first branch is frequency-doubled and used for side-band cooling and interrogation of the Yb atoms (the "heart" of the atomic clock) for long-term stability. The second branch is sent to the ultra low expansion (ULE) cavity (see Fig. 3.4) for PDH stabilization for short-term stability. The third branch is used to lock the frequency comb to the stabilized clock laser (see Sec. 3.3).

The locked comb is used to transfer the stability of the clock laser to an 1560 nm communication laser to disseminate the stable signal out of the lab by a long-range optical fiber link (see Sec. 2.4). A FNC system compensates for the noise induced by the optical fibers to achieve a stable signal at the fiber output.

CHAPTER 3. EXPERIMENTAL REALIZATION OF THE YB CLOCK SYSTEM

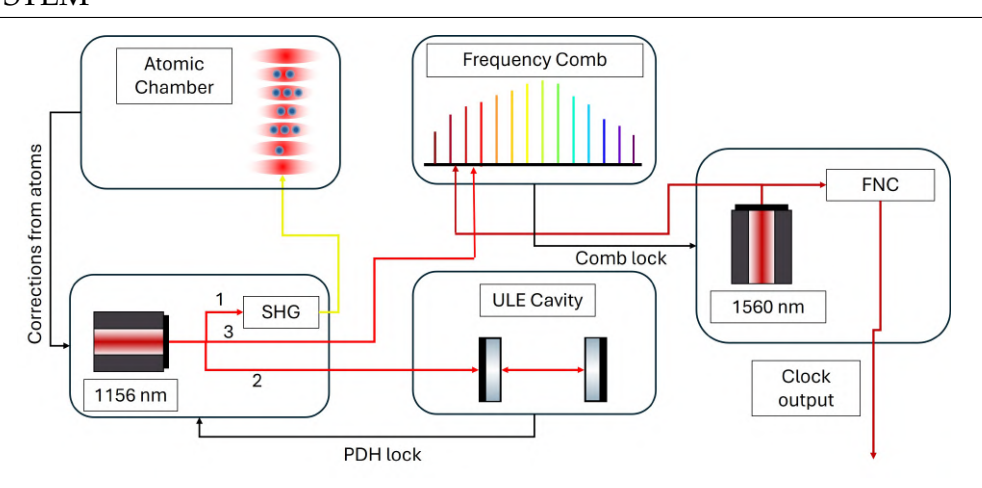


Figure 3.1: Block diagram of the BGU Yb clock. The light of the clock laser at 1156 nm is split into three channels: 1. the laser frequency is doubled by second harmonic generation (SHG) to the clock transition at 578 nm (see Fig. 2.1) that is used to interrogate the cooled Yb atoms trapped in an optical lattice; 2. the laser is locked to a ULE optical cavity for short-term stability and linewidth narrowing; 3. the stable laser output is used to lock a femtosecond OFC. The stable comb is then used to lock a 1560 nm communication laser. To disseminate the stable clock output from the lab, a FNC system is installed on the outbound optical fiber to compensate for phase noise along the optical fiber connecting the lab to a remote user. The FNC system acts upon the signal reflected from a remote system to compensate for errors accumulated over the long fiber length to the client, as discussed in Sec. 2.4.

3.2 Clock Laser Lock Scheme and Operation

The clock laser light is produced by an external cavity diode laser (ECDL) operating at 1156nm, which is doubled to 578nm for the Yb clock transition, as shown in Fig. 3.1. The laser we use in this experiment is MOGLabs CEL, a 'cateye' design external cavity diode laser (ECDL) at 1156 nm [83]. The laser system consists of an external cavity formed between the rear reflecting surface of a semi-conductor laser diode and a cateye output coupler mounted on a piezoelectric (PZT) actuator as depicted in Fig. 3.2. A high-efficiency ultra-narrow filter is inserted into the external cavity to select a single external cavity mode. The rotation angle of the filter determines the transmitted wavelength, which is back-reflected by the output coupler into the laser diode. Scanning of the laser frequency is performed by applying a periodic AC voltage on the PZT that changes the external

cavity length.

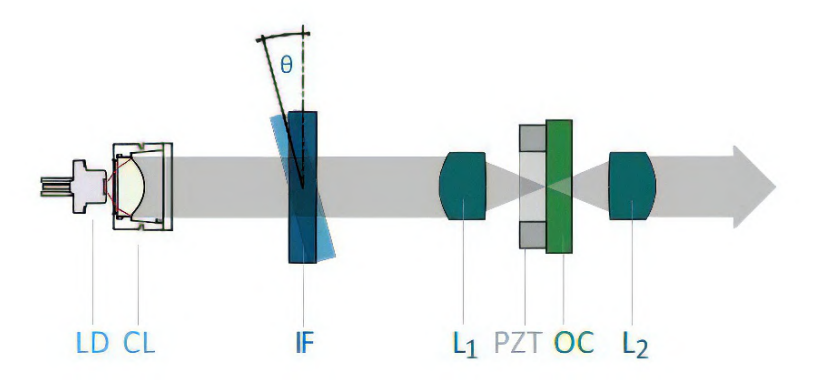


Figure 3.2: Schematic of a cateye external cavity diode laser (ECDL). Light from the laser diode (LD) is collimated by using a lens (CL) and then filtered via an angled bandpass interference filter (IF), through L1 the cateye lens to the partially transmitting output coupler (oc) and recollimated by lens L2 [83].

The optical setup of the clock laser system is depicted in Fig. 3.3. The output wavelength is at 1156nm which is frequency doubled in a periodically poled lithium niobate (PPLN) waveguide (Advr, RSH-T0578-P98FSALO-190510551) to generate 578 nm for probing the clock transition. The 578 nm and 1156 nm wavelengths are separated using a dichroic mirror (DM). The 1156 nm radiation is directed to the ULE cavity for linewidth narrowing and to the frequency comb for frequency comparisons and dissemination.

We use three AOMs (G & H 3080 197) for various operations on the 1156 nm lines. The first AOM is in a double-pass configuration, driven at 80 MHz using a home-made voltage controlled oscillator. Corrections to long-term drifts identified by probing the atoms are digitally added to the frequency of this AOM. The other two AOMs are used to stabilize the phase and amplitude of the mini-links between the laser and the cavity/comb. The drivers of these two AOMs are based on direct digital synthesis (DDS) oscillators (MOGLabs, ARF).

CHAPTER 3. EXPERIMENTAL REALIZATION OF THE YB CLOCK SYSTEM

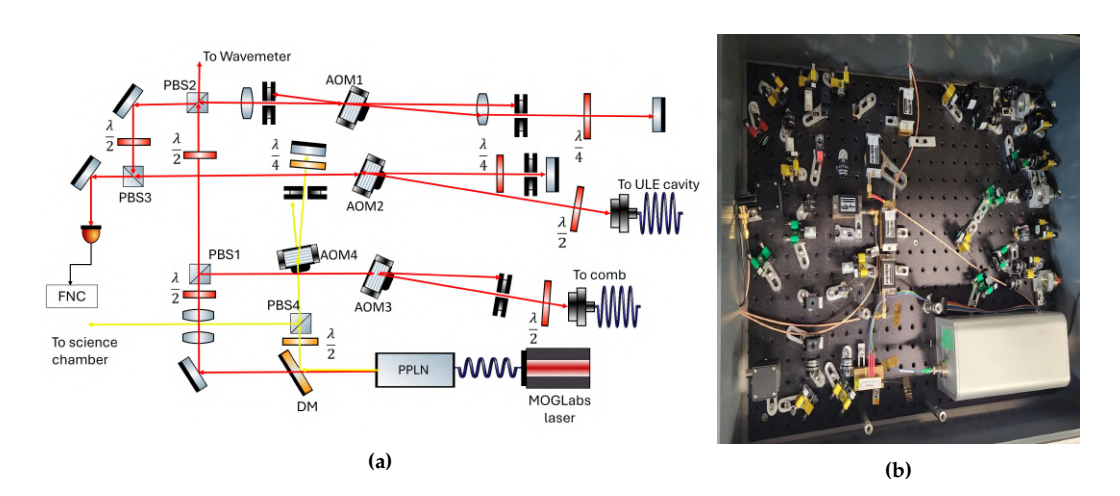


Figure 3.3: (a) The clock laser optical system: light from the laser (lower-right corner) is fiber coupled to a PPLN waveguide for SHG. The output of the PPLN, containing both the original and the doubled frequencies, is filtered by a DM. The doubled frequency at 578 nm is directed through a double pass AOM setup and reflected towards the science chamber. The fundamental frequency beam is split into two parts by a polarizing beam splitter (PBS) after a beam-shape correction telescope. The part that is transmitted through PBS1 is split again at PBS2 with a small part of the intensity directed into a wavemeter. Most of the intensity is directed through a double-pass AOM1 to introduce the frequency correction from the atoms to the laser. The reflected beam is transferred through PBS2 and directed by PBS3 to the ULE cavity system (see Fig. 3.4) after passing through AOM2 as a part of the cavity mini-link FNC system. The reflected part from PBS1 is directed to the frequency comb through AOM3. (b) A photo of the described setup.

The PDH technique (see Sec. 2.2.2) is applied for stabilizing the laser. We use a 30 cm long ULE cavity (Stable Laser Systems), which is isolated against acoustic noise and external vibrations [57], see Fig. 3.4c. The optical setup inside the acoustic enclosure is shown in Fig. 3.4.

Light from the clock laser system is transferred via an optical fiber to the cavity enclosure. The beam is divided by a 30:70 T:R beam splitter. The light is partially reflected back to the fiber through a second reflection from the beam splitter and used for fiber noise cancellation (see Sec 3.2.3). The transmitted light from the second pass in the beam splitter is measured by PD1 (Thorlabs, DET10N2), see Fig. 3.4a.

CHAPTER 3. EXPERIMENTAL REALIZATION OF THE YB CLOCK SYSTEM

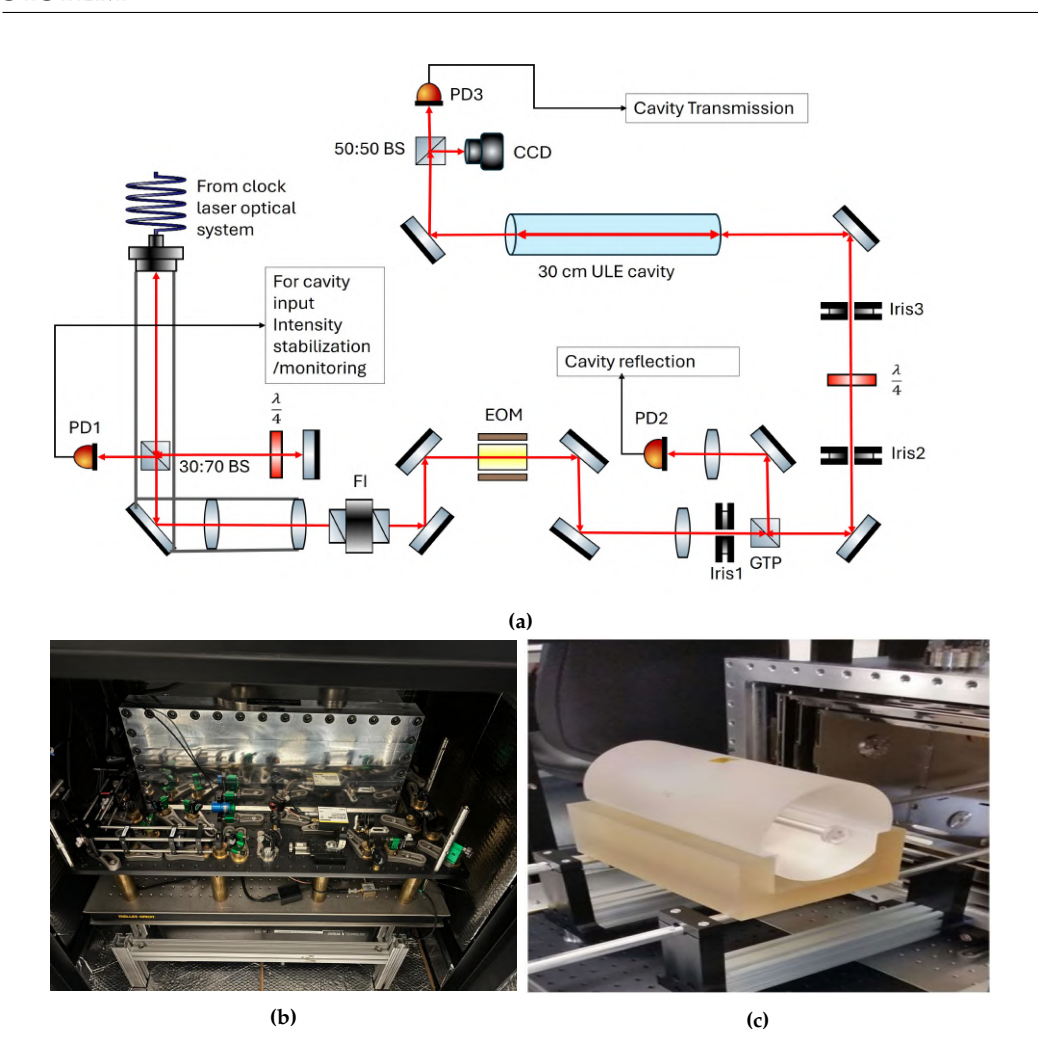


Figure 3.4: (a) The optical system inside the cavity enclosure box: light arrives from the clock laser system (Fig. 3.3) via an optical fiber (top-left corner) and is collimated and split by a 30:70 (T:R) beam splitter. The reflected part is redirected back to the fiber for FNC and intensity monitoring by PD1. The transmitted part is directed through a cage-system mounted telescope for mode-matching with the cavity. Next, the beam passes through a Faraday isolator (FI) and an EOM for phase modulation. The beam is then focused with a lens for mode-matching to the ULE cavity. A series of three irises are used for spatial alignment of the beam. The beam reflected from the cavity facet is directed by a Glan-Thompson polarizer (GTP) to a fast and amplified PD2. The light transmitted through the cavity is split equally between PD3 for measuring the cavity transmission and a CCD camera to identify the spatial mode of the beam. (b) A photo of the optical system inside the cavity enclosure box. (c) The 30 cm long ULE cavity on top of a Zerodur base mount is inserted into the vacuum chamber. The vacuum chamber contains three shielding layers for high-temperature stabilization and acoustic noise isolation [57].

Stabilizing the light intensity in the cavity setup is important to eliminate

error signal fluctuations caused by variations in the intra-cavity optical power. PD1 is used to monitor the light intensity in the cavity enclosure box. Fig. 3.5 shows a one-hour recording of the intensity measured by PD1. The results show a stable average intensity level of 58.2 μ W with a standard deviation of 0.2 μ W over this period. A $3 \cdot 10^{-3}$ relative uncertainty is a good starting point. For a typical optical cavity system, power-dependent frequency shifts are on the order of $10 \, \text{Hz}/\mu$ W [84], so we can assume that we are now at a level of 2 Hz fluctuations. We chose to refrain from actively stabilizing the intensity at this point, as it is not the most detrimental noise source to the clock laser stability (see the following sections), although the option to implement active intensity stabilization in the future exists.

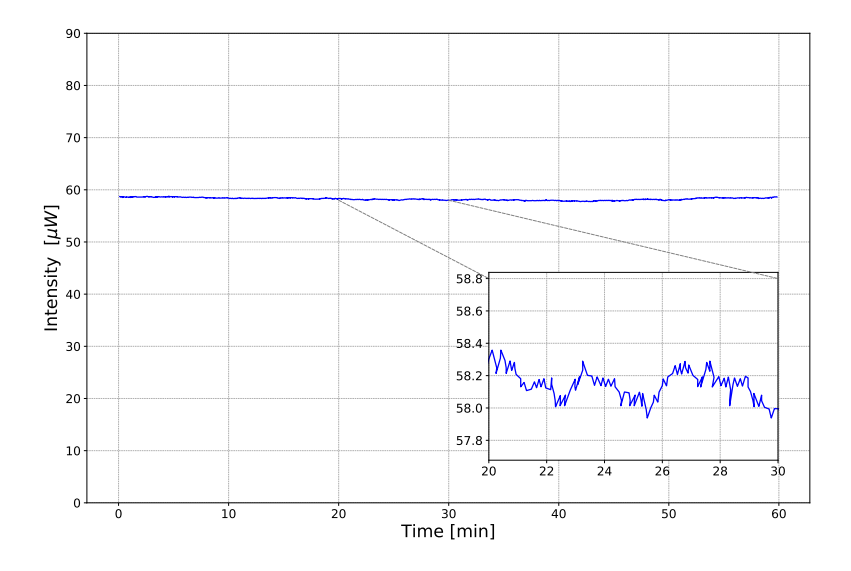


Figure 3.5: Monitoring of the ULE cavity incident light intensity over 1 hour. inset: a 10-minute section of the measurement. The average intensity over the measurement period was $58.2 \, \mu W$ with a standard deviation of $0.2 \, \mu W$.

The initial alignment of a high-finesse cavity is a challenging task. The parameters of the ULE cavity are described in the M.Sc. Thesis of Yosef Bivas [57]. It should be noted that one of the mirrors of the cavity is flat while the other is curved. In addition, the area of coating on the mirrors is

not large (a 10 mm hole drilled in the glass block defines the transmission channel). If the laser beam misses the coatings, a high transmission signal will appear. Because the cavity is placed inside a large vacuum chamber, it is impossible to view the incident point on the cavity. The alignment procedure starts with mode-matching the shape of the laser beam to ensure overlap with the TEM₀₀ cavity mode, as described in [57]. This is done using a telescope and a convex lens to align the beam waist with the cavity input flat mirror. Next, we used two steering mirrors to scan the area near the center of the vacuum chamber window until a back reflection is identified. The mirrors are then used to obtain an overlap of the back reflection with the incident beam. At this stage, the laser frequency is slowly scanned at about 5 Hz (sufficiently slow to obtain a measurable on-resonance transmission signal, as monitored by PD2 (in Fig. 3.4a).

Care must be taken to avoid high power, which may damage the coating on the cavity mirrors. Hence, during the alignment stages, the power is kept below 1 mW while scanning, then further reduced to $\sim 50~\mu\text{W}$ when approaching alignment and before locking. When alignment is improved, fringes can be detected (averaging of the transmission signal can be very useful). During this stage, we monitor the fringes and amplify the signal (x200) using a low-noise preamplifier (SRS, SR560) set to function as a band-pass filter (1-10 kHz). This amplifier is used for peak detection.

A tedious and iterative procedure is performed to improve the alignment on both the vertical and the horizontal axes. The number of fringes is reduced during this procedure due to the excitation of a smaller number of modes. Eventually, the TEM₀₀ mode is practically the only mode left (see Fig. 3.6a), as can be verified using a CCD camera (see Fig. 3.8b). For a very high-finesse cavity like this, it is practically impossible to observe the cavity modes using the camera unless the laser frequency is locked, as the linewidth is very narrow and the transmission pulses are weak. The photo shown in Fig. 3.8b was taken when the cavity was locked. After cavity alignment, the reflected beam is directed into a fast PD (Thorlabs, DET10N2, later replaced with Menlo Systems, FPD510-FS-NIR).

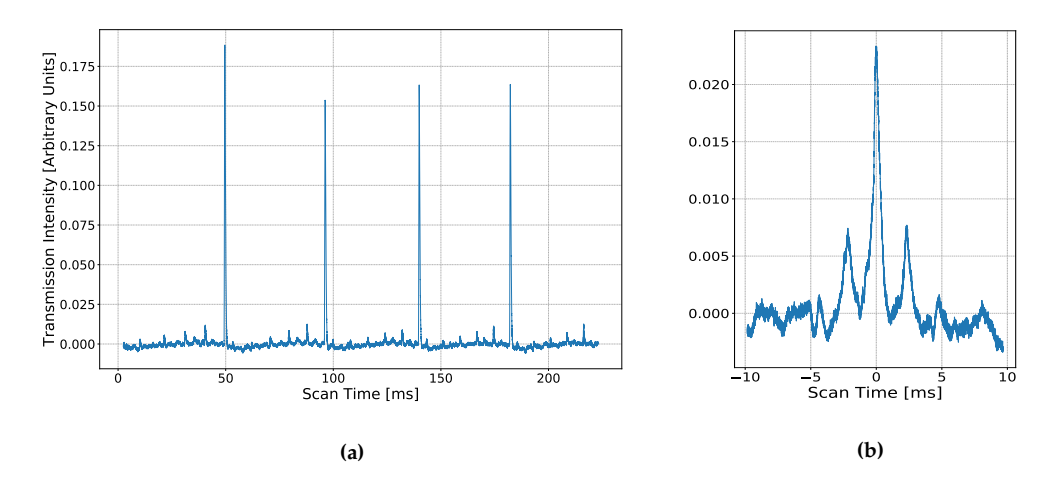


Figure 3.6: Light transmission intensity through the cavity. (a) The laser frequency scan range is about 5 cavity FSRs (for our 30 cm long cavity the FSR is 0.5 GHz). The TEM_{00} mode is prominent compared with higher-order spatial modes. Transmission was recorded with an oscilloscope, averaging over 16 samples. (b) A single TEM_{00} mode with sidebands created by the EOM. Data were taken with a 16 sample average.

The PDH setup is shown in Fig. 3.7. The EOM (Photonics Technologies, EOM-01-20-IR) is used for sideband generation (see Fig. 3.6b). It is modulated by a function generator (Rigol, DG 1022Z) which gets a reference signal of 10 MHz from a Rb timebase (AccuBeat, AR76). The function generator has two phase-coherent outputs. The output of the first channel is amplified using an RF amplifier (MiniCircuits, ZHL-3A+) to drive the EOM. The output of the second channel is connected to the LO port of the mixer (MiniCircuits, ZAD-3+). We use an amplified fast PD (Menlo systems, PFD-510-FS-NIR) to detect the interference of the reflected instantaneous laser light with the leakage long-lived field oscillating in the cavity. The PD output is connected to a DC block filter (MiniCircuits, BLK-18-S+). The DC block output is amplified $\times 20$ using a home-made circuit and connected to the RF port of the mixer. We connect a low-pass filter (MiniCircuits, SLP-5+) to the IF port of the mixer. The output after the filter has the error-signal information enters the fast servo controller (FSC) system (MOGLabs, FSC). The FSC unit has fast and slow outputs. The slow output operates on the piezo crystal, which controls the length of the

laser's external filter cavity. To generate the necessary lock bandwidth, the current has to be directly injected into the laser diode. This is achieved by the B1240 headboard, which has a current modulation bandwidth of 4 MHz.

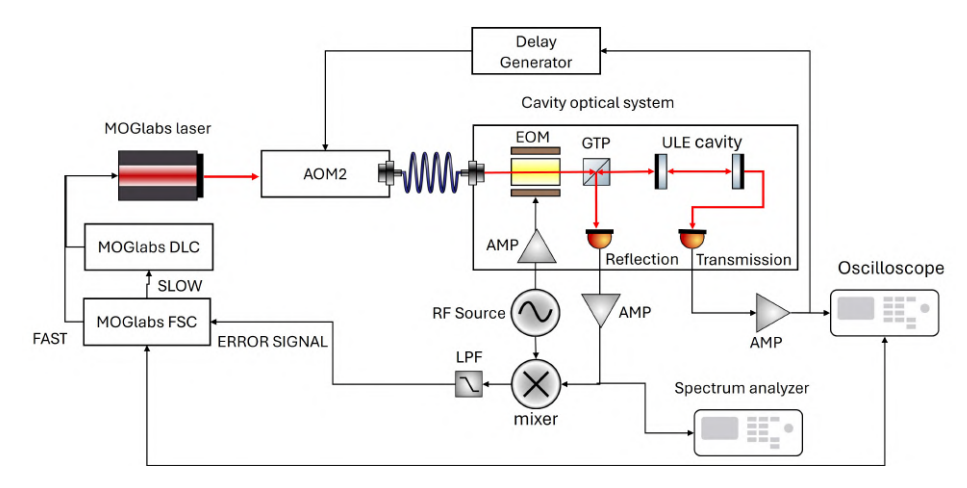


Figure 3.7: The PDH electronic system: the MOGLabs ECDL (upper-left corner) is controlled by the diode laser controller (MOGLabs, DLC202), and the servo feedback loop is managed by the fast servo controller (MOGLabs FSC100). The laser beam passes through the clock optical system, further discussed in Fig. 3.3. The laser in the cavity enclosure passes through the system shown in Fig. 3.4. The light transmitted from the cavity is directed to a PD. The signal is amplified using Toptica miniScan 102 (later replaced by SRS, SR560) and divided between an oscilloscope and the Digital Delay Generator (SRS, DG645) activated as a shutter for the signal of AOM2 of Fig. 3.3a, for the cavity ringdown measurement (see Sec. 3.2.1). The cavity reflection beam is directed to a different PD whose signal is amplified and connected to the mixer.

Once the cavity is properly aligned, the scan range can be reduced to concentrate on one of the temporal fringes. The phase shift between the two modulation channels needs to be adjusted to achieve a symmetrical error signal. A stable PDH lock can be obtained by carefully adjusting the PID parameters. After an initial lock is achieved, the stability is maximized by fine-tuning the lock parameters.

3.2.1 Evaluation of the Cavity Finesse

For the ring-down measurement [66, 69], a pulse delay generator (SRS, DG645) controlled the RF amplitude fed into AOM2 (see Fig. 3.3a) RF

amplitude, and hence the first-order beam which goes to the cavity. After achieving a lock, the delay generator was triggered by a threshold PD voltage, switching off AOM2 for a period of time, sufficiently long to allow all the light circulating in the cavity to escape, but also short enough to preserve the frequency lock.

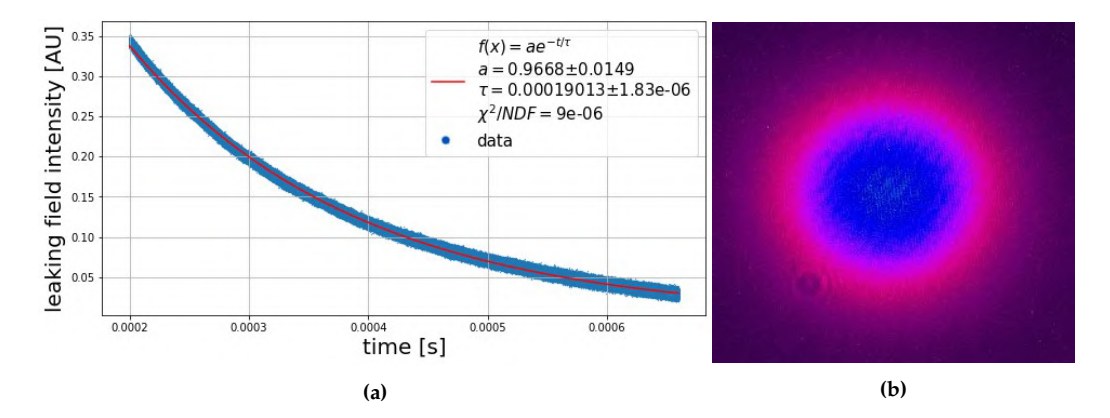


Figure 3.8: (a) Exponential fit for the cavity ring-down measurement. The decay time is used to calculate the cavity finesse according to Eq. 2.12. (b) The TEM_{00} mode transmission through the cavity.

The results of the cavity ring-down measurement are shown in Fig. 3.8a, to which an exponential function was fitted to determine the resonator lifetime and thus obtain the value of the cavity finesse:

$$\tau = 190 \pm 2 \,\mu\text{s}$$

$$\Rightarrow \mathcal{F} = 597000 \pm 6000 \tag{3.1}$$

The linewidth of the cavity resonance fringe can be calculated from the obtained finesse according to Eqs. 2.7,2.12:

$$\nu_{FSR} \approx 0.5 \,\text{GHz} \implies \delta \nu \approx 1 \,\text{kHz}$$
 (3.2)

The finesse value obtained from the cavity ring-down measurement (\sim 600,000) deviates from the "ideal" theoretical cavity finesse (628,000) [57] by only about 5%. Taking into account errors in the reflectivity values and other loss mechanisms that contribute to lifetime reduction, this value is

close enough to the best we could have expected and is comparable with the best cavities used for Yb clocks [33, 59, 63].

3.2.2 Comparison to an Independent Stable Laser System

In May 2023 we compared our locked laser to an independent laser system (Menlo Systems, ORS-Mini ultra-stable laser systems), which we had on loan for two weeks. The comparison of the two systems consisted of locking a frequency comb to the ORS-Mini and measuring the beat note between the locked clock laser and the closest comb tooth, which encodes the stability of the ORS-Mini. The result of this measurement is shown in Fig. 3.9. Close to the end of the loan period, the beat note detection unit (BDU) malfunctioned, so unfortunately we could not further optimize our system.

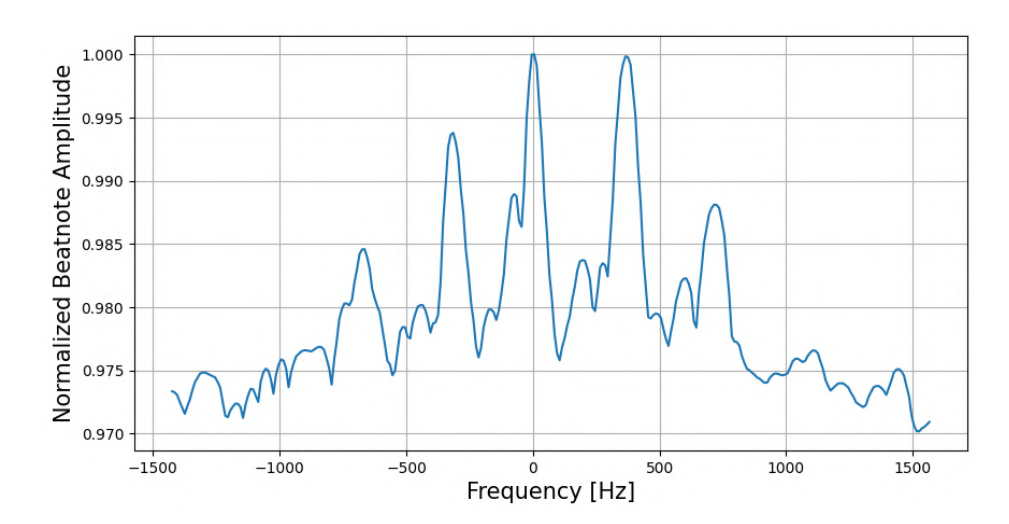


Figure 3.9: The beat note measured between our clock laser and the Menlo Systems ORS-Mini ultra-stable laser system. The results show a profile of a few separated "fingers" with a linewidth on the order of 100 Hz. The beat note profile was recorded by a Rhode and Schwarz FSP spectrum analyzer with a resolution and video bandwidth of 30 Hz and a sweep time of 2 s. The center frequency is arbitrarily chosen as the maximum point of the graph.

The results of this measurement were thus unsatisfactory, leading to the implementation of several changes. As we noticed a significant phase-

noise induced by the optical fiber we decided to implement a fiber noise cancellation system, as described in the following section. We also replaced the fiber collimator mount feeding light to the cavity enclosure box by a more robust one. The optical path following the fiber collimator was redesigned using a cage system. We also replaced the PD that measures the reflection from the cavity with an AC-coupled one (Menlo Systems, FPD510-FS-NIR) to prevent saturation of the PD.

3.2.3 Cavity Mini-Link

One of the modifications made in our system - after the disappointing results achieved for the ORS comparison - is the application of a fiber noise cancellation system to the optical fiber connecting the clock laser optical system (see Fig. 3.3a) and cavity enclosure box (see Fig. 3.4). The system is similar to the one shown in Fig. 2.7 without the output AOM, which is not needed for such a short distance (5 m).

Observing the beat note between the local arm and the retro-reflected signal from the cavity system showed a wide linewidth of $\sim 10~\rm kHz$, pointing to a large phase noise accumulation. We identified the source of this problem to be a mechanical coupling between the protective tubing that transferred mechanical vibrations from the surrounding to the fiber medium. Once the fiber was removed from the tubing, the beat note signal linewidth was significantly reduced.

To realize the FNC system to the cavity mini-link, the beat note is measured by a fast PD (EOT, ET-3000A) and amplified (Mini-Circuits, ZHL1-2W-S+). The amplified signal is mixed with a 160 MHz signal synthesized by a function generator (SRS, SG384), the mixer (Mini-circuits, ZAD-3+) is low-pass filtered (Mini-circuits, BLP-1.9+) and the resulting error signal is the input to a PID controller (SRS, SIM960) that generates a correction signal modulating the AOM frequency.

Fig. 3.10a shows the effect of the noise cancellation system on the beat note, as can be seen by the difference between the locked (orange) and un-

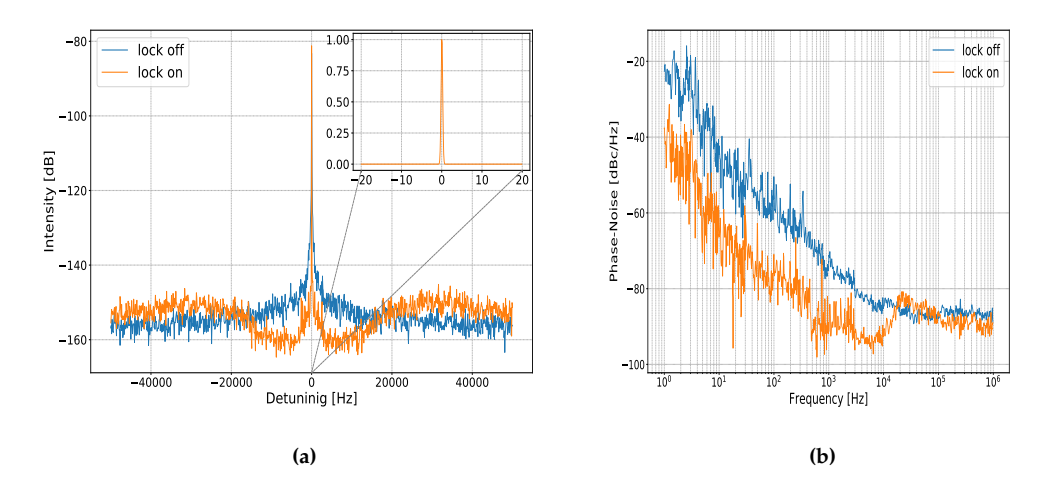


Figure 3.10: (a) The recorded beat note of the cavity mini-link FNC system sowing a 100 kHz frequency span around the central peak at 160 MHz. The locked signal (orange) possesses lower noise characteristics at lower frequencies relative to the carrier, compared to the unlocked signal (blue). At higher frequencies signal servo bumps at ~ 20 kHz are observed. The data were taken with a 10 Hz radio/video bandwidth spectrum analyzer. Inset: a zoomed-in view of the locked beat note, with a 40 Hz frequency span. The linewidth of the beat signal is limited by the device resolution of 1 Hz bandwidth. (b) The relative phase noise of the locked and unlocked signals. The stabilization of the signal reduces the phase noise by about 20 dBc/Hz for low frequencies below about 20 kHz mark.

locked (blue) data. The locked signal linewidth is limited by the resolution of the measuring spectrum analyzer (Rohde & Schwarz, FSV3013) of 1 Hz. The one-sided relative phase noise level of the two signals is shown in Fig. 3.10b. A suppression of \sim 20 dBc/Hz is achieved for frequencies up to 20 kHz relative to the carrier frequency.

We believe that this issue was detrimental for comparison to the ORS system. By decoupling the fiber from the noisy environment and applying the noise cancellation system, we have significantly improved the linewidth. However, a quantitative determination of the linewidth can be done only when a comparable narrow linewidth source is available in the future (see Ch. 4).

3.3 The Comb System

The optical frequency comb installed in our system (Menlo Systems, FC1500-250-ULN) is shown in Fig. 3.11. It consists of the electronics rack and the optical setup which is mounted on a breadboard stationed on a vibration isolation stage (Minus K, VIBRAPLANE). In our system, the OFC laser is an erbium-doped fiber laser in a "Figure 9" configuration [85]. The comb light is generated by the seed laser and directed to the different amplifiers and BDUs via optical fibers - either internally through the comb modules, as in the case of the f-2f interferometer (as explained by Eq. 2.23) - or externally, leading the signals to the external BDUs. The f-2f module is used to extract the CEO frequency, while the repetition rate is extracted from the laser module. To lock the comb, the two RF signals for the repetition rate and the CEO frequency are locked by a designated servo loop controller (Menlo Systems, SYNCRO). The electronics rack contains the locking electronics for the comb signals as well as an oscilloscope and frequency counter for monitoring and tracking the measured frequencies.

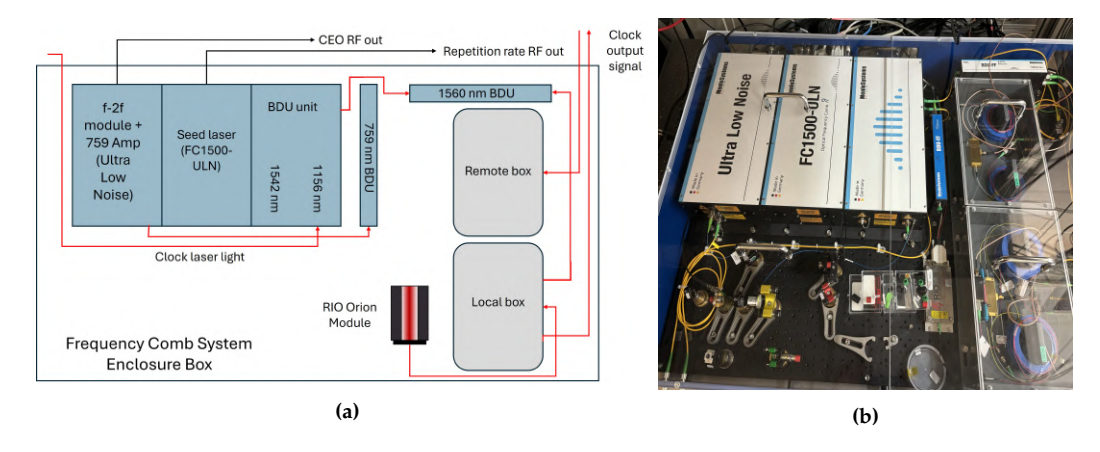


Figure 3.11: The optical frequency comb setup installed in our lab. (a) Schematics of the system. The comb light is generated in the box designated FC1500-ULN (second box, top-left). The left-hand box includes the f-2f interferometer for the CEO locking and the amplifier for the 759 nm light for the matching BDU. The right-hand box includes two BDU units: at 1156 nm for the clock laser and 1542 nm for comparison to an independent laser system (see Sec. 3.2.2). The 1560 nm BDU (top-right) is connected to the clock output link noise cancellation system (see Sec. 3.4) (b) Picture of the described setup.

The locking of the repetition rate can be done in two ways as described in Sec. 2.3 - either by using a stable RF standard, such as an Rb clock which we have in our lab (AccuBeat, AR76) - or by using a stable optical frequency.

3.3.1 Lock to a Radio Frequency Reference

Fig. 3.12 shows a four-hour long measurement of the comb parameter (f_{ceo} and f_{rep}) while locked to an RF reference. The measurement was done by the comb internal frequency counter with a gate time of 1 s.

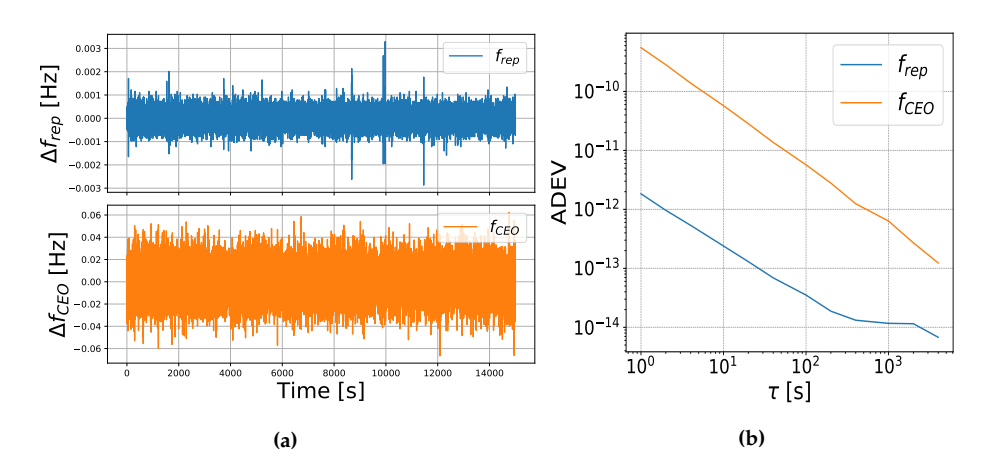


Figure 3.12: Locking the comb to an RF signal. (a) Deviation from the set frequency of the CEO frequency ($\bar{f}_{ceo} = 35 \text{MHz}$) and the repetition rate ($\bar{f}_{rep} = 250 \text{MHz}$) over a four-hour period. (b) The ADEV of the signals.

The stability of the measured signal is limited by that of the microwave clock. These results demonstrate the ability of the OFC to transfer the stability of the locking reference signal to each tooth. Thus, in the future, when we use the clock laser as an optical reference to lock the comb parameters, each comb tooth will be as stable as the optical clock signal.

3.4 Long-Distance Fiber link Noise Cancellation System

As was briefly explained in Sec. 2.4.1 we need to stabilize fiber links, especially if they are long. The clock output dissemination system is shown in Fig. 3.13. The 1560 nm communication laser (Rio, ORION Module) is fiber-coupled to the FNC system. The system is divided into two separate boxes: the local box (see Fig. 3.13b), including the local arm of the inteferometer and the AOM modulating the signal, and the remote box (see Fig. 3.13c), which is in charge of retro-reflecting the signal back to the lab to compensate for the accumulation of phase noise along the long fiber link. The remote box will be placed in a distant location, but at this stage it is located in our lab adjacent to the local box (see Fig. 3.11b) for first evaluation of the BGU-TAU link (see Fig. 3.14).

In the local box, light is divided into two parts. The smaller part (10%) is directed to the frequency comb BDU to achieve a beat note with the adjacent comb tooth. The beat note is used to generate an error signal to stabilize the Rio laser, using the comb locking electronics (Menlo Systems, SYNCRO LLE), transferring the stability of the comb to the laser. When the frequency comb is stabilized by the clock laser, we transfer the comb stability to the Rio laser, making it the output signal of the clock. The major part of the beam is directed to the BGU Communication Center - which is connected to the communication network, through the noise cancellation system. The setup for the fiber-link noise cancellation system is similar to the basic scheme described in Sec. 2.4.1, with a major difference of being completely fiber coupled. The local arm of the interferometer (10% of the beam intensity) is split from the output signal and reflected from a Faraday mirror back to the splitter and to a PD. The rest of the laser light is directed into an AOM (G & H, Fiber-Q® PM 1550 nm 40 MHz (AMTIR)). The 1storder diffracted beam (at 40 MHz modulation frequency) is directed to the output fiber link through a polarization controller. In the "Remote" box, a second AOM2 modulates the light frequency again for identification. Half of the intensity is directed to a Faraday mirror and reflected back to the fiber through AOM2 and to the local box. The beam is modulated again by AOM1 for a total frequency shift of 160 MHz (40 MHz for each AOM pass), mixed with the local arm and the beat note is measured by a PD (Thorlabs, DET08CFC).

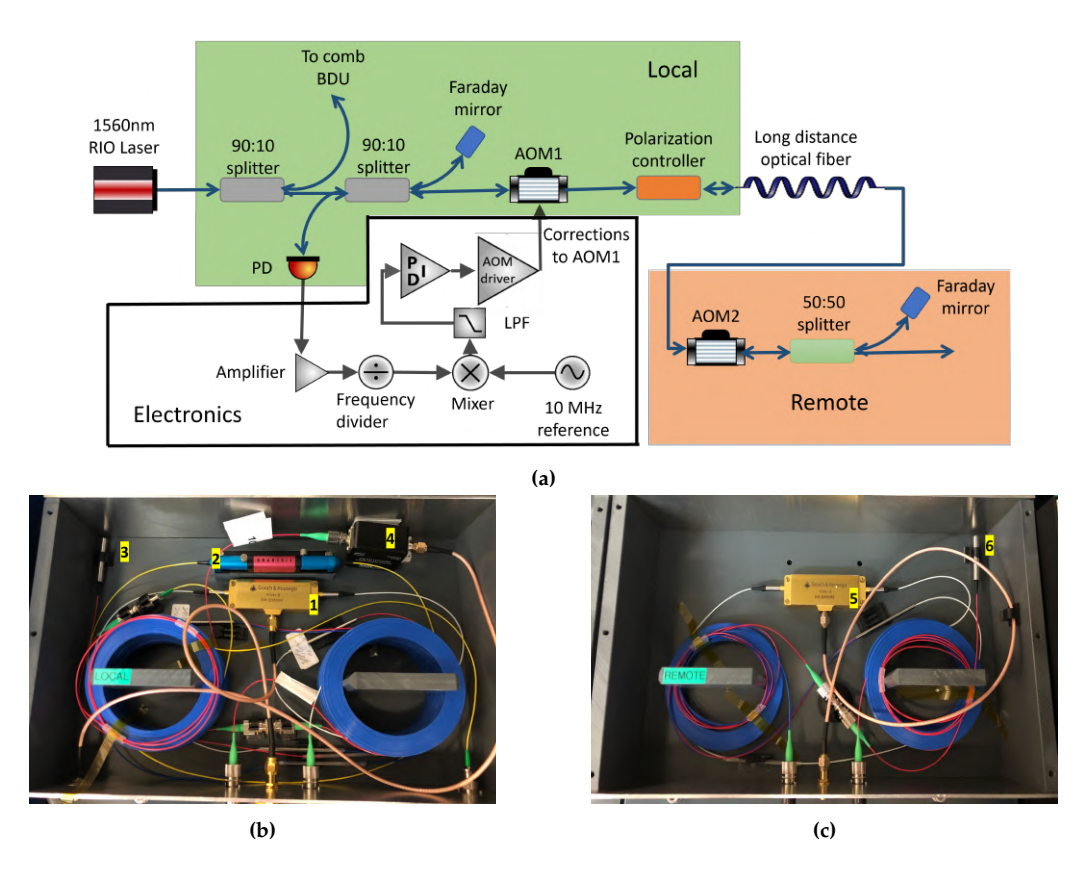


Figure 3.13: (a) The fiber-link noise cancellation system scheme. (b) The "local" box; a fiber-coupled laser is fed to the system, and the beam is split twice. First, a small part of the beam is directed to lock the laser to a stable frequency comb. The major part splits again and passes through AOM1 (1) and a polarization controller (2) before coupling to the external optical fiber. A small part of the original beam propagates towards a Faraday mirror (3) and then recombines with a retro-reflected beam from the output fiber to achieve an interferometer. The beat note between the two beams is detected by a fast PD (4). (c) The "Remote" box; the light from the fiber passes through AOM2 (5) to differentiate the beam that passes through the full pass from unwanted reflections produced by optical components along the path. The AOM2 output is split into the lownoise output, and a second Faraday mirror (6) is used to reflect the beam back to the "local" box. The measured beat note is amplified, divided, and mixed with a 10 MHz reference. The mixer output is low-pass filtered to create an error signal, which is fed to a PID servo to control the AOM1 driver.

The measured beat signal is amplified (Mini-Circuits, ZHL-1-2W-S+) and the frequency is divided by a factor of 16 (Analog Devices, HMC394LP4). The signal is then compared to a stable RF oscillator at 10 MHz by an RF mixer. The mixer output is low-pass filtered to generate the error signal which is fed to the PID controller (SRS, SIM960). The controller output modulates the frequency that drives AOM1 generated by a function generator (Keysight, 33600A) to apply the correction signal to the laser light.

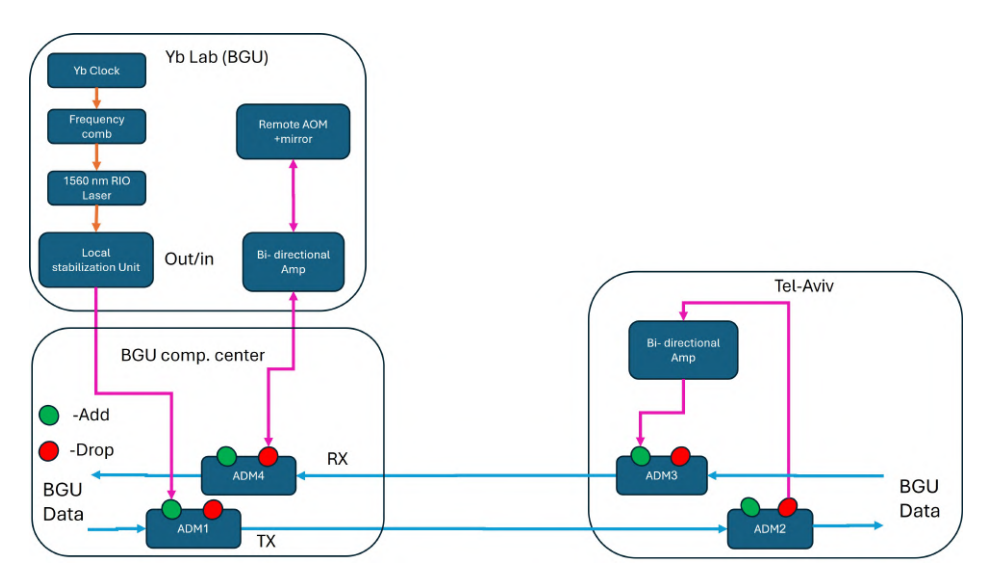


Figure 3.14: The block diagram of the BGU-TAU fiber loop: the stable laser output signal of the Yb OLC is directed through the FNC system local box (Fig. 3.13b) to the BGU Communications Center. There the clock light is fed to the transmission communication fiber - TX via the Add port of add-drop multiplexer (ADM)1 in the BGU communications center. In Tel Aviv the clock signal is extracted from the Drop port of ADM2, amplified by a bi-directional optical amplifier and added to the BGU receiving fiber - RX, through ADM3. From the RX fiber the clock signal is extracted by ADM4 and directed to the Yb Lab to pass through a second bi-directional amplifier and to the FNC systems remote box (Fig. 3.13c).

From our lab, the stable laser light from the local box output is directed to the BGU Communications Center to transmit the clock signal over the inter-university fiber network (see Fig. 1.2). Fig. 3.14 presents the planned system for the BGU-TAU link connection, as a prerequisite to the connection between our Yb clock and the Sr ion clock stationed at the Weizmann Institute. The light from our lab is directed to the BGU TX fiber (commu-

CHAPTER 3. EXPERIMENTAL REALIZATION OF THE YB CLOCK SYSTEM

nication transmission fiber) by an ADM (Fibernet, OADM), which allows the addition and extraction of our laser signal from the communication network infrastructure without disruption of the regular communication signal.

In Tel Aviv, the clock laser light is extracted from the TX fiber through the ADM2 drop port. To overcome the attenuation of the laser intensity while propagating through the long fiber (~100 km) a bi-directinal amplifier (Keopsys, CEFA-C-BD) is stationed in Tel-Aviv. The amplified beam is directed to the BGU RX fiber (receiving communication fiber) via the ADM3 Add port. At BGU, the signal is extracted via the ADM4 Drop port and directed to the Yb clock lab, where the light is amplified again and inserted to the remote box.

As of the day of writing this thesis we have installed the two ADMs in the BGU Communication Center and are in contact with the Tel-Aviv Center for installation of our devices and on-site measurements. Work is delayed due to manpower issues.

4 Summary and Outlook

This thesis summarizes the work I performed in the framework of my M.Sc. on the ¹⁷¹Yb OLC, focusing on laser stabilization and frequency dissemination. The goal of this project is to generate a stable laser signal that is the "heart" of an optical atomic clock and to disseminate its output without impacting the signal stability.

To achieve a stable and narrow-linewidth clock laser, I constructed and operated the clock laser optical system (see Fig. 3.3a) and performed locking and stabilization to a high-finesse cavity (see Sec. 3.2.1). I operated the optical frequency comb system, stabilized it to an RF reference (see Sec. 3.3.1) and an optical reference, and performed a comparison between our laser and an independent stable laser system (see Sec. 3.2.2). The comparison pointed to a high noise level in our laser system. To eliminate this noise, I built and optimized the cavity mini-link FNC system (see Fig. 3.2.3) and successfully reduced the noise level induced by light propagating through the optical fiber from the optical table to the ULE cavity. In order to successfully complete the work on this subject, the frequency comb still needs to be locked to the stable clock laser - and a second comparison to a different laser should be carried out to verify our laser stability.

In the field of frequency dissemination, I designed the FNC system that is installed in our lab (see Sec. 3.4) and the infrastructure to link our lab to the inter-university fiber communication network. Following the work summarized here, the following tasks need to be completed in the near future:

- 1. Lock the communication laser to the stable comb.
- 2. Stabilize the optical fiber link from the lab to the BGU Communications Center.
- 3. Install ADMs and a bi-directional amplifier in Tel-Aviv.
- 4. Introduce our laser light to the BGU TX fiber and measure the signal output in Tel-Aviv.
- 5. Stabilize the BGU-Tel-Aviv fiber link.

When completed, these tasks will allow us to connect and compare our clock with the ion clock being developed at the Weizmann Institute.

In addition, major progress is currently achieved in our lab in the area of trapping and cooling of Yb atoms. Moreover, a large purchase order has been placed for multiple RF frequency standards, including hydrogen maser and cesium beam atomic clocks. These devices would replace the current atomic clock used as an RF standard for the frequency comb and the other devices in our system.

When the above tasks are complete, along with the full operation of the clock, we will be able to use our system as a source for a stable frequency standard, contributing to precise timekeeping in Israel and to fundamental science.

Bibliography

- [1] I. Alonso, C. Alpigiani, B. Altschul, H. Araújo, G. Arduini, J. Arlt, L. Badurina, A. Balaz, S. Bandarupally, B. Barish, M. Barone, M. Barsanti, S. Bass, A. Bassi, B. Battelier, C. Baynham, Q. Beaufils, A. Belic, J. Bergé, and E. Zupanič, "Cold atoms in space: Community workshop summary and proposed road-map," *EPJ Quantum Technol.*, vol. 9, 2022.
- [2] M. Pizzocaro, P. Thoumany, B. Rauf, F. Bregolin, G. Milani, C. Clivati, G. A. Costanzo, F. Levi, and D. Calonico, "Absolute frequency measurement of the ${}^{1}S_{0}$ ${}^{3}P_{0}$ transition of 171 Yb," *Metrologia*, vol. 54, 2017.
- [3] A. Trabesinger, "Nobel prize 2005: Glauber, Hall and Hänsch," *Nat. Phys.*, vol. 1, 2005.
- [4] C. W. Chou, D. B. Hume, T. Rosenband, and D. J. Wineland, "Optical clocks and relativity," *Sci.*, vol. 329, 2010.
- [5] W. F. McGrew, X. Zhang, R. J. Fasano, S. A. Schäffer, K. Beloy, D. Nicolodi, R. C. Brown, N. Hinkley, G. Milani, M. Schioppo, T. H. Yoon, and A. D. Ludlow, "Atomic clock performance enabling geodesy below the centimetre level," *Nat.*, vol. 564, 2018.
- [6] N. Huntemann, B. Lipphardt, C. Tamm, V. Gerginov, S. Weyers, and E. Peik, "Improved limit on a temporal variation of m_p/m_e from comparisons of Yb⁺ and Cs atomic clocks," *Phys. Rev. Lett.*, vol. 113, 2014.

- [7] V. Schkolnik, D. Budker, O. Fartmann, V. Flambaum, L. Hollberg, T. Kalaydzhyan, S. Kolkowitz, M. Krutzik, A. Ludlow, N. Newbury, C. Pyrlik, L. Sinclair, Y. Stadnik, I. Tietje, J. Ye, and J. Williams, "Optical atomic clock aboard an Earth-orbiting space station (OACESS): enhancing searches for physics beyond the standard model in space," *Quantum. Sci. Technol.*, vol. 8, 2022.
- [8] T. P. Heavner, S. R. Jefferts, E. A. Donley, J. H. Shirley, and T. E. Parker, "NIST-F1: recent improvements and accuracy evaluations," *Metrologia*, vol. 42, 2005.
- [9] J. Lodewyck, "On a definition of the SI second with a set of optical clock transitions," *Metrologia*, vol. 56, 2019.
- [10] F. Riehle, "Towards a redefinition of the second based on optical atomic clocks," C. R. Phys., vol. 16, 2015.
- [11] I. Ushijima, M. Takamoto, M. Das, T. Ohkubo, and H. Katori, "Cryogenic optical lattice clocks," *Nat. Photonics*, vol. 9, 2015.
- [12] X. Zhang, K. Beloy, Y. S. Hassan, W. F. McGrew, C.-C. Chen, J. L. Siegel, T. Grogan, and A. D. Ludlow, "Subrecoil clock-transition laser cooling enabling shallow optical lattice clocks," *Phys. Rev. Lett.*, vol. 129, 2022.
- [13] D. Allan, "Statistics of atomic frequency standards," *Proc. IEEE*, vol. 54, 1966.
- [14] W. Riley and D. Howe, "Handbook of frequency stability analysis," 2008.
- [15] A. D. Ludlow, M. M. Boyd, J. Ye, E. Peik, and P. O. Schmidt, "Optical atomic clocks," *Rev. Mod. Phys.*, vol. 87, 2015.
- [16] F. Riehle, Frequency Standards: Basics and Applications. Wiley-VCH, 2004.

- [17] I. D. Leroux, N. Scharnhorst, S. Hannig, J. Kramer, L. Pelzer, M. Stepanova, and P. O. Schmidt, "On-line estimation of local oscillator noise and optimisation of servo parameters in atomic clocks," *Metrologia*, vol. 54, 2017.
- [18] I. D. Leroux, N. Scharnhorst, S. Hannig, J. Kramer, L. Pelzer, M. Stepanova, and P. O. Schmidt, "On-line estimation of local oscillator noise and optimisation of servo parameters in atomic clocks," *Metrologia*, vol. 54, 2017.
- [19] W. M. Itano, J. C. Bergquist, J. J. Bollinger, J. M. Gilligan, D. J. Heinzen, F. L. Moore, M. G. Raizen, and D. J. Wineland, "Quantum projection noise: Population fluctuations in two-level systems," *Phys. Rev. A*, vol. 47, 1993.
- [20] S. Weyers, V. Gerginov, M. Kazda, J. Rahm, B. Lipphardt, G. Dobrev, and K. Gibble, "Advances in the accuracy, stability, and reliability of the PTB primary fountain clocks," *Metrologia*, vol. 55, 2018.
- [21] S. Häfner, S. Falke, C. Grebing, S. Vogt, T. Legero, M. Merimaa, C. Lisdat, and U. Sterr, " 8×10^{-17} fractional laser frequency instability with a long room-temperature cavity," *Opt. Lett.*, vol. 40, 2015.
- [22] A. Derevianko, K. Gibble, L. Hollberg, N. R. Newbury, C. Oates, M. S. Safronova, L. C. Sinclair, and N. Yu, "Fundamental physics with a state-of-the-art optical clock in space," *Quantum Sci. Technol.*, vol. 7, 2022.
- [23] A. Aeppli, K. Kim, W. Warfield, M. S. Safronova, and J. Ye, "Clock with 8×10^{-19} systematic uncertainty," *Phys. Rev. Lett.*, vol. 133, 2024.
- [24] J. Tiedau, M. V. Okhapkin, K. Zhang, J. Thielking, G. Zitzer, E. Peik, F. Schaden, T. Pronebner, I. Morawetz, L. T. De Col, F. Schneider, A. Leitner, M. Pressler, G. A. Kazakov, K. Beeks, T. Sikorsky, and T. Schumm, "Laser excitation of the Th-229 nucleus," *Phys. Rev. Lett.*, vol. 132, 2024.

- [25] J. D. Roslund, A. Cingöz, W. D. Lunden, G. B. Partridge, A. S. Kowligy, F. Roller, D. B. Sheredy, G. E. Skulason, J. P. Song, J. R. Abo-Shaeer, and M. M. Boyd, "Optical clocks at sea," *Nat.*, vol. 628, 2024.
- [26] K. H. Leung, B. Iritani, E. Tiberi, I. Majewska, M. Borkowski, R. Moszynski, and T. Zelevinsky, "Terahertz vibrational molecular clock with systematic uncertainty at the 10⁻¹⁴ level," *Phys. Rev. X*, vol. 13, 2023.
- [27] J. He, B. Pasquiou, R. G. Escudero, S. Zhou, M. Borkowski, and F. Schreck, "Coherent three-photon excitation of the strontium clock transition," 2024.
- [28] R. Grimm, M. Weidemüller, and Y. Ovchinnikov, "Optical dipole traps for neutral atoms," *Adv. At. Mol. Opt. Phy.*, vol. 42, 2000.
- [29] K. Beloy, M. I. Bodine, T. Bothwell, S. M. Brewer, S. L. Bromley, J.-S. Chen, J.-D. Deschênes, S. A. Diddams, R. J. Fasano, T. M. Fortier, Y. S. Hassan, D. B. Hume, D. Kedar, C. J. Kennedy, I. Khader, A. Koepke, D. R. Leibrandt, H. Leopardi, A. D. Ludlow, W. F. McGrew, W. R. Milner, N. R. Newbury, D. Nicolodi, E. Oelker, T. E. Parker, J. M. Robinson, S. Romisch, S. A. Schäffer, J. A. Sherman, L. C. Sinclair, L. Sonderhouse, W. C. Swann, J. Yao, J. Ye, X. Zhang, and Boulder Atomic Clock Optical Network (BACON) Collaboration*, "Frequency ratio measurements at 18-digit accuracy using an optical clock network," *Nat.*, vol. 591.
- [30] N. D. Lemke, A. D. Ludlow, Z. W. Barber, T. M. Fortier, S. A. Diddams, Y. Jiang, S. R. Jefferts, T. P. Heavner, T. E. Parker, and C. W. Oates, "Spin-1/2 optical lattice clock," *Phys. Rev. Lett.*, vol. 103, 2009.
- [31] V. Formichella, G. Signorile, T. T. Thai, L. Galleani, M. Pizzocaro, I. Goti, S. Condio, C. Clivati, M. Risaro, F. Levi, D. Calonico, and I. Sesia, "Year-long optical time scale with sub-nanosecond capabilities," *Optica*, vol. 11, 2024.

- [32] T. Kobayashi, D. Akamatsu, Y. Hisai, T. Tanabe, H. Inaba, T. Suzuyama, F.-L. Hong, K. Hosaka, and M. Yasuda, "Uncertainty evaluation of an 171Yb optical lattice clock at nmij," *IEEE T. Ultrason. Ferr.*, vol. 65, 2018.
- [33] A. Zhang, Z. Xiong, X. Chen, Y. Jiang, J. Wang, C. Tian, Q. Zhu, B. Wang, D. Xiong, L. He, L. Ma, and B. Lyu, "Ytterbium optical lattice clock with instability of order 10⁻¹⁸," *Metrologia*, vol. 59, 2022.
- [34] H. Kim, M.-S. Heo, C. Y. Park, D.-H. Yu, and W.-K. Lee, "Absolute frequency measurement of the 171Yb optical lattice clock at kriss using TAI for over a year," *Metrologia*, vol. 58, 2021.
- [35] M. Barbiero, D. Calonico, F. Levi, and M. G. Tarallo, "Optically loaded strontium lattice clock with a single multi-wavelength reference cavity," *IEEE Trans. Instrum. Meas.*, vol. 71, 2022.
- [36] R. Tyumenev, M. Favier, S. Bilicki, E. Bookjans, R. L. Targat, J. Lodewyck, D. Nicolodi, Y. L. Coq, M. Abgrall, J. Guéna, L. D. Sarlo, and S. Bize, "Comparing a mercury optical lattice clock with microwave and optical frequency standards," New J. Phys., vol. 18, 2016.
- [37] K. Yamanaka, N. Ohmae, I. Ushijima, M. Takamoto, and H. Katori, "Frequency ratio of Hg199 and Sr87 optical lattice clocks beyond the si limit," *Phys. Rev. Lett.*, vol. 114, 2015.
- [38] A. Yamaguchi, M. Safronova, K. Gibble, and H. Katori, "Narrow-line cooling and determination of the magic wavelength of cd," *Phys. Rev. Lett.*, vol. 123, 2019.
- [39] M. Steinel, H. Shao, M. Filzinger, B. Lipphardt, M. Brinkmann, A. Didier, T. E. Mehlstäubler, T. Lindvall, E. Peik, and N. Huntemann, "Evaluation of a ⁸⁸Sr⁺ optical clock with a direct measurement of the blackbody radiation shift and determination of the clock frequency," *Phys. Rev. Lett.*, vol. 131, 2023.

- [40] P. Dubé, A. A. Madej, and B. Jian, "Sr+ single-ion clock," *J. Phys. Conf. Ser.*, vol. 723, 2016.
- [41] C. Sanner, N. Huntemann, R. Lange, C. Tamm, E. Peik, M. S. Safronova, and S. G. Porsev, "Optical clock comparison for lorentz symmetry testing," *Nat.*, vol. 567, 2019.
- [42] T. Rosenband, D. Hume, P. Schmidt, C. Chou, A. Brusch, L. Lorini, W. Oskay, R. Drullinger, T. Fortier, J. Stalnaker, S. Diddams, W. Swann, N. Newbury, W. Itano, D. Wineland, and J. Bergquist, "Frequency ratio of Al+ and Hg+ single-ion optical clocks; metrology at the 17th decimal place," *Sci.*, vol. 319, 2008.
- [43] J. Cao, J. Yuan, S. Wang, P. Zhang, Y. Yuan, D. Liu, K. Cui, S. Chao, H. Shu, Y. Lin, S. Cao, Y. Wang, Z. Fang, F. Fang, T. Li, and X. Huang, "A compact, transportable optical clock with 1×10^{-17} uncertainty and its absolute frequency measurement," *Appl. Phys. Lett.*, vol. 120, 2022.
- [44] S. M. Brewer, J.-S. Chen, A. M. Hankin, E. R. Clements, C. W. Chou, D. J. Wineland, D. B. Hume, and D. R. Leibrandt, "²⁷Al⁺ quantum-logic clock with a systematic uncertainty below 10⁻¹⁸," *Phys. Rev. Lett.*, vol. 123, 2019.
- [45] W. McGrew, X. Zhang, H. Leopardi, R. Fasano, D. Nicolodi, K. Beloy, J. Yao, J. Sherman, S. Schaffer, J. Savory, R. Brown, S. Romisch, C. Oates, T. Parker, T. Fortier, and A. Ludlow, "Towards the optical second: verifying optical clocks at the si limit," *Optica*, vol. 6, 2019.
- [46] N. Ohmae, F. Bregolin, N. Nemitz, and H. Katori, "Direct measurement of the frequency ratio for Hg and Yb optical lattice clocks and closure of the Hg/Yb/Sr loop," *Opt. Express*, vol. 28, 2020.
- [47] IUCC, "Network Services Israel's National Research & Education Network (NREN)." https://www.iucc.ac.il/en/infrastructuretechnologies/networking/.

- [48] D. Husmann, L.-G. Bernier, M. Bertrand, D. Calonico, K. Chaloulos, G. Clausen, C. Clivati, J. Faist, E. Heiri, U. Hollenstein, A. Johnson, F. Mauchle, Z. Meir, F. Merkt, A. Mura, G. Scalari, S. Scheidegger, H. Schmutz, M. Sinhal, S. Willitsch, and J. Morel, "Si-traceable frequency dissemination at 1572.06 nm in a stabilized fiber network with ring topology," Opt. Express, vol. 29, 2021.
- [49] C. Clivati, R. Aiello, G. Bianco, C. Bortolotti, P. D. Natale, V. D. Sarno, P. Maddaloni, G. Maccaferri, A. Mura, M. Negusini, F. Levi, F. Perini, R. Ricci, M. Roma, L. S. Amato, M. S. de Cumis, M. Stagni, A. Tuozzi, and D. Calonico, "Common-clock very long baseline interferometry using a coherent optical fiber link," *Optica*, vol. 7, 2020.
- [50] F. Guillou-Camargo, V. Ménoret, E. Cantin, O. Lopez, N. Quintin, E. Camisard, V. Salmon, J.-M. L. Merdy, G. Santarelli, A. Amy-Klein, P.-E. Pottie, B. Desruelle, and C. Chardonnet, "First industrial-grade coherent fiber link for optical frequency standard dissemination," *Appl. Opt.*, vol. 57, 2018.
- [51] H. Schnatz, O. Terra, K. Predehl, T. Feldmann, T. Legero, B. Lipphardt, U. Sterr, G. Grosche, T. W. Hansch, R. Holzwarth, T. Udem, Z. Lu, L. Wang, W. Ertmer, J. Friebe, A. Pape, E.-M. Rasel, M. Riedmann, and T. Wubbena, "Phase-coherent frequency comparison of optical clocks using a telecommunication fiber link," in 2009 IEEE International Frequency Control Symposium Joint with the 22nd European Frequency and Time forum, 2009.
- [52] C. Clivati, M. Pizzocaro, E. Bertacco, S. Condio, G. Costanzo, S. Donadello, I. Goti, M. Gozzelino, F. Levi, A. Mura, M. Risaro, D. Calonico, M. Tønnes, B. Pointard, M. Mazouth-Laurol, R. Le Targat, M. Abgrall, M. Lours, H. Le Goff, L. Lorini, P.-E. Pottie, E. Cantin, O. Lopez, C. Chardonnet, and A. Amy-Klein, "Coherent optical-fiber link across italy and france," *Phys. Rev. Appl.*, vol. 18, 2022.
- [53] M. Schioppo, J. Kronjäger, A. Silva, R. Ilieva, J. W. Paterson, C. F. A.

Baynham, W. Bowden, I. R. Hill, R. Hobson, A. Vianello, M. Dovale-Álvarez, R. A. Williams, G. Marra, H. S. Margolis, A. Amy-Klein, O. Lopez, E. Cantin, H. Álvarez-Martínez, R. Le Targat, P. E. Pottie, N. Quintin, T. Legero, S. Häfner, U. Sterr, R. Schwarz, S. Dörscher, C. Lisdat, S. Koke, A. Kuhl, T. Waterholter, E. Benkler, and G. Grosche, "Comparing ultrastable lasers at 7×10^{-17} fractional frequency instability through a 2220 km optical fibre network," *Nat. Commun.*, vol. 13, 2022.

- [54] Y. B. Band and A. Vardi, "Collisional shifts in optical-lattice atom clocks," *Phys. Rev. A*, vol. 74, 2006.
- [55] M. Takamoto, I. Ushijima, M. Das, N. Nemitz, T. Ohkubo, K. Yamanaka, N. Ohmae, T. Takano, T. Akatsuka, A. Yamaguchi, and H. Katori, "Frequency ratios of Sr, Yb, and Hg based optical lattice clocks and their applications," *C. R. Phys.*, vol. 16, 2015.
- [56] A. V. Taichenachev, V. I. Yudin, C. W. Oates, C. W. Hoyt, Z. W. Barber, and L. Hollberg, "Magnetic field-induced spectroscopy of forbidden optical transitions with application to lattice-based optical atomic clocks," *Phys. Rev. Lett.*, vol. 96, 2006.
- [57] Y. Bivas, "¹⁷¹Yb Optical Lattice Clock in BGU," Master's thesis, Ben Gurion University of the Negev, 2021.
- [58] W. D. Phillips and H. Metcalf, "Laser deceleration of an atomic beam," *Phys. Rev. Lett.*, vol. 48, Mar 1982.
- [59] G. Milani, "Realization of advanced ¹⁷¹Yb optical lattice frequency standard". PhD thesis, Istituto Nazionale di Ricerca Metrologica, 2018.
- [60] H. Katori, T. Ido, and M. Kuwata-Gonokami, "Optimal Design of Dipole Potentials for Efficient Loading of Sr Atoms," J PHYS SOC JPN, vol. 68, 1999.
- [61] H. Katori, "Optical lattice clocks and quantum metrology," *Nat. Photonics*, vol. 5, 2011.

- [62] A. Derevianko and H. Katori, "Colloquium: Physics of optical lattice clocks," *Rev. Mod. Phys.*, vol. 83, 2011.
- [63] N. D. Lemke, "Optical Lattice Clock with Spin-1/2 Ytterbium Atoms". PhD thesis, University of Colorado Boulder, 2012.
- [64] N. Ismail, C. C. Kores, D. Geskus, and M. Pollnau, "Fabry-pérot resonator: spectral line shapes, generic and related airy distributions, linewidths, finesses, and performance at low or frequency-dependent reflectivity," *Opt. Express*, vol. 24, 2016.
- [65] S. Kasap, *Optoelectronics and photonics : principles and practices*. Prentice Hall, 2001.
- [66] J. H. van Helden, R. Peverall, and G. A. D. Ritchie, *Cavity Enhanced Techniques Using Continuous Wave Lasers*, ch. 2. John Wiley Sons, Ltd, 2009.
- [67] G. P. Agrawal, "Noise in semiconductor lasers and its impact on optical communication systems," in *Laser Noise* (R. Roy, ed.), vol. 1376, International Society for Optics and Photonics, SPIE, 1991.
- [68] E. D. Black, "An introduction to pound–drever–hall laser frequency stabilization," *Am. J. Phys.*, vol. 69, 2001.
- [69] R. W. Fox, C. W. Oates, and L. W. Hollberg, "1. stabilizing diode lasers to high-finesse cavities," in *Cavity-Enhanced Spectroscopies* (R. D. van Zee and J. P. Looney, eds.), vol. 40 of *Experimental Methods in the Physical Sciences*, Academic Press, 2003.
- [70] R. W. P. Drever, J. L. Hall, F. V. Kowalski, J. Hough, G. M. Ford, A. J. Munley, and H. Ward, "Laser phase and frequency stabilization using an optical resonator," *Appl. Phys. B: Lasers Opt.*, vol. 31, 1983.
- [71] D. Bersanetti, "Lock Acquisition & Commissioning of the Advanced Virgo detector," *PoS Proc. Sci.*, vol. NEUTEL2017, 2018.

- [72] M. Abramowitz, Handbook of Mathematical Functions, With Formulas, Graphs, and Mathematical Tables,. USA: Dover Publications, Inc., 1974.
- [73] N. Picqué and T. W. Hänsch, "Frequency comb spectroscopy," *Nat. Photonics*, vol. 13, 2019.
- [74] M. Ahmadi, B. X. R. Alves, C. J. Baker, W. Bertsche, A. Capra, C. Carruth, C. L. Cesar, M. Charlton, S. Cohen, R. Collister, S. Eriksson, A. Evans, N. Evetts, J. Fajans, T. Friesen, M. C. Fujiwara, D. R. Gill, J. S. Hangst, W. N. Hardy, M. E. Hayden, C. A. Isaac, M. A. Johnson, J. M. Jones, S. A. Jones, S. Jonsell, A. Khramov, P. Knapp, L. Kurchaninov, N. Madsen, D. Maxwell, J. T. K. McKenna, S. Menary, T. Momose, J. J. Munich, K. Olchanski, A. Olin, P. Pusa, C. Ø. Rasmussen, F. Robicheaux, R. L. Sacramento, M. Sameed, E. Sarid, D. M. Silveira, G. Stutter, C. So, T. D. Tharp, R. I. Thompson, D. P. van der Werf, and J. S. Wurtele, "Characterization of the 1S–2S transition in antihydrogen," *Nat.*, vol. 557, 2018.
- [75] J. Braunfelds, R. Murnieks, T. Salgals, I. Brice, T. Sharashidze, I. Lyashuk, A. Ostrovskis, S. Spolitis, J. Alnis, J. Porins, and V. Bobrovs, "Frequency comb generation in WGM microsphere based generators for telecommunication applications," *Quantum Electron.*, vol. 50, 2020.
- [76] Y.-J. Kim, B. Chun, Y. Kim, S. Hyun, and S.-W. Kim, "Generation of optical frequencies out of the frequency comb of a femtosecond laser for DWDM telecommunication," *Laser Phys. Lett.*, vol. 7, 2010.
- [77] T. Briles, J. Stone, T. Drake, D. Spencer, C. Fredrick, Q. Li, D. Westly, B. Ilic, K. Srinivasan, S. Diddams, and S. Papp, "Interlocking kerrmicroresonator frequency combs for microwave to optical synthesis," *Opt. Lett.*, vol. 43, 2018.
- [78] L. Duan, "General treatment of the thermal noises in optical fibers," *Phys. Rev. A*, vol. 86, 2012.

- [79] A. Bengtsson, "Experimental Implementation of a Fiber Noise Cancellation System for Slow Light Laser Locking," Master's thesis, Lund University, 2017.
- [80] L.-S. Ma, P. Jungner, J. Ye, and J. L. Hall, "Delivering the same optical frequency at two places: accurate cancellation of phase noise introduced by an optical fiber or other time-varying path," *Opt. Lett.*, vol. 19, 1994.
- [81] A. Franzen, "ComponentLibrary: a free vector graphics library for optics gwoptics.org." https://www.gwoptics.org/ComponentLibrary/.
- [82] S. Donadello, C. Clivati, A. Govoni, L. Margheriti, M. Vassallo, D. Brenda, M. Hovsepyan, E. K. Bertacco, R. Concas, F. Levi, A. Mura, A. Herrero, F. Carpentieri, and D. Calonico, "Seismic monitoring using the telecom fiber network," *Commun. Earth Environ.*, vol. 5, 2024.
- [83] D. J. Thompson and R. Scholten, "Narrow linewidth tunable external cavity diode laser using wide bandwidth filter.," *Rev. Sci. Instrum.*, vol. 83, 2012.
- [84] W. Qi, Y. Jiang, X. Li, L. Jin, Z. Bi, and L. Ma, "Study on the sensitivity of optical cavity length to light power fluctuation," *Chin. Opt. Lett.*, vol. 14, 2016.
- [85] G. Liu, S. Ou, Q. Zhang, M. Zhang, X. Li, and Q. Bao, "All-polarization-maintaining linear fiber laser mode-locked by nonlinear polarization evolution with phase bias," *Opt. Laser. Technol.*, vol. 142, 2021.